

Omar Eduardo Jiménez López

Development of biomechatronic devices for measurement of wrenches occurring in animal and human prehension

Berichte aus der Biomechatronik

Herausgegeben von Prof. Dr. Hartmut Witte

Fachgebiet Biomechatronik an der TU Ilmenau

Band 9

Development of biomechatronic devices for measurement of wrenches occurring in animal and human prehension

Omar Eduardo Jiménez López



Universitätsverlag Ilmenau
2014

Impressum

Bibliografische Information der Deutschen Nationalbibliothek

Die Deutsche Nationalbibliothek verzeichnet diese Publikation in der Deutschen Nationalbibliografie; detaillierte bibliografische Angaben sind im Internet über <http://dnb.d-nb.de> abrufbar.

Diese Arbeit hat der Fakultät für Maschinenbau der Technischen Universität Ilmenau als Dissertation vorgelegen.

Tag der Einreichung: 10. Dezember 2010
1. Gutachter: Univ.-Prof. Dipl.-Ing. Dr. med. (habil.) Hartmut Witte
(Technische Universität Ilmenau)
2. Gutachter: Univ.-Prof. Dr.-Ing. habil. Thomas Fröhlich
(Technische Universität Ilmenau)
3. Gutachter: Univ.-Prof. Dr. phil. nat. (habil.) Reinhard Blickhan
(Friedrich Schiller Universität Jena)
Tag der Verteidigung: 23. Mai 2011

Technische Universität Ilmenau/Universitätsbibliothek

Universitätsverlag Ilmenau

Postfach 10 05 65
98684 Ilmenau
www.tu-ilmenau.de/universitaetsverlag

Herstellung und Auslieferung

Verlagshaus Monsenstein und Vannerdat OHG
Am Hawerkamp 31
48155 Münster
www.mv-verlag.de

ISSN 1865-9136 (Druckausgabe)
ISBN 978-3-86360-102-7 (Druckausgabe)
URN urn:nbn:de:gbv:ilm1-2011000555

Titelfoto: Dipl.-Biol. Helga Schulze | Bochum

Danksagung

Ich bedanke mich ganz herzlich beim CONSEJO NACIONAL DE CIENCIA Y TECNOLOGÍA (CONACYT) und bei der SECRETARÍA DE EDUCACIÓN PÚBLICA (SEP) für die Unterstützung und Ausbildungsförderung während meiner Promotion.

Besonders bedanke ich mich bei meinem Doktorvater Univ.-Prof. Dipl.-Ing. Dr. med. (habil.) Hartmut Witte für seine wissenschaftliche Betreuung, insbesondere für seine fachliche Unterstützung und sein persönliches Engagement.

Ich bedanke mich ganz herzlich bei meinen kompetenten Kollegen, für ihre Zeit, die Teilhabe an ihrem Wissen und ihre Freundschaft. Insbesondere bei Dr. Emanuel Andrada, Dr. Jörg Mämpel, Carlos Bernardo Schymansky, Emiliano José Guitart Piguillem, Jörg Schade, Danja Voges, Dr. Cornelius Schilling, Kerstin Schmidt, Dr. Beate Schlütter, Juan Carlos Moreno Sagaon, Silvia Lehman und Dr. Ulrike Fröber.

Anerkennung gebührt meiner Ehefrau Elizabeth Aguilar für Ihre stete Unterstützung, Dank für ihre Liebe und ihren Beistand. Gleichfalls bedanke ich mich sehr bei Jorge Amado González Whittinham, Dr. Alejandra López de González Whittinham und Amadita für ihre Freundschaft und Unterstützung.

Vielen Dank auch an Ruben, María Laura, Leo, Meche, Bartolomé, Diego, Teodora, Andrea, Anna und Sasha.

Acknowledgments

I want to express my gratitude to the brilliant and talented colleagues who have shared with me their time, knowledge and friendship for my five years in Germany. Your support was invaluable for this Dissertation.

Also I thank my advisor, Prof. Dr. Hartmut Witte, for the great support, patience and friendship that I received from him. His human side is equal in size as his scientific knowledge.

I thank my family for the love expressed in these five years, especially for the love expressed by my wife Elizabeth; my mother and my brothers.

I thank the CONSEJO NACIONAL DE CIENCIA Y TECNOLOGÍA (CONACYT) for its support and grant during this time.

As well I thank the SECRETARÍA DE EDUCACIÓN PÚBLICA (SEP) for its financial support.

Finally, I want to express my special thanks to Jorge González, Alejandra López, Amadita, Carlos Bernardo Schymansky, Emiliano José Guitart Piguillem, Emanuel Andrada, Jörg Schade, Jörg Mämpel, Danja Voges, Juan Carlos Moreno Sagaon, Silvia Lehman and Ulrike Fröber for their invaluable personal, technical and scientific support.

Zusammenfassung

Titel: Entwicklung biomechatronischer Geräte für die Bestimmung von Kraftgrößen bei der Beobachtung tierischer und menschlicher Prehension.

Verfasser: Omar Eduardo Jiménez López

Biomechatronik und speziell Biosensoren unterstützen auf der Grundlage biologischer Inspiration das Entstehen neuer Anwendungen in der ganzen Spanne vom Fahrzeugbau bis zur Bio-Robotik. Dabei werden Mechatronik, technologisches Wissen, Bionik und Biologie miteinander kombiniert. "There is a market trend towards the use of intelligent sensors. In the past the main reasons for this have been increased measurement accuracy, programmability, decreased inventory cost from the larger turndown available, and a decreased maintenance cost for self-diagnostics." (Expertise, 1997).

Im speziellen Anwendungsfall der Kletterrobotik erlaubt der Einsatz von biokompatiblen Kraftgrößen-Sensoren die Etablierung dynamischer Modelle der Fortbewegung von Tieren als bionische Basis biologischer Inspiration. Ergonomische Gestaltung von Griffen bedarf fundierter Kenntnisse über die vektoriellen Greifkräfte. Im Rahmen dieser Arbeit wurden daher miniaturisierte 6 DOF-Kraftgrößensensoren entwickelt, die als aktive Knoten eines Sensor-Netzwerks firmieren können.

Multisensorenanwendungen können die räumliche und zeitliche Auflösung eines Messaufbaus deutlich steigern. "Durch die Verknüpfung der Signale mehrerer Sensoren lassen sich die Zuverlässigkeit und der Anwendungsbereich vergrößern und die Signalqualität deutlich steigern. Neben einer Verbesserung der Signalqualität ergeben sich durch die Nutzung der in der Steuerung vorhanden Positions- und Richtungsinformation neue Anwendungen" (Adam, 2000).

Dabei wird in der vorgelegten Arbeit Wert auf eine Detaillierung der Darstellung des Entwurfsprozesses gelegt, um in Zeiten fragmentierten Publizierens durch Dokumentation an einem Orte verallgemeinerbares Erfahrungswissen für die Entwicklung biokompatibler Kraftgrößensensoren zu sichern.

Abstract

Title: Development of biomechatronic devices for measurement of wrenches occurring in animal and human prehension

Author: Omar Eduardo Jiménez López

Biomechatronics and biosensors dedicate their ability to support new applications inspired from nature on automotive, exoskeleton systems (Hwang & Moo, 2009), intelligent humanoid robots (Wu & Wu, 2010) and robotics (Qiakang Liang, 2010), with a combination of technical knowledge, biology, bionics and mechatronics. "There is a market trend towards the use of intelligent sensors. In the past the main reasons for this have been increased measurement accuracy, programmability, decreased inventory cost from the larger turndown available, and a decreased maintenance cost for self-diagnostics." (Expertise, 1997).

On the other hand, for climbing machines (Mämpel, Koch & Köhring, 2009) biomechatronics discovers important descriptive models of locomotion of monkeys, rats or chameleons in which each aspect of the animal's movement is clearly defined (Witte, Lutherdt & Schilling, 2004). Adaptable and ergonomic grips used in cars, motorcycles and trains need a deep and vast supportive knowledge from human grasping. This knowledge cannot be won without the help of experimentation in animal and human prehension to produce enough evidence and valid data about the biological structures (Jeffrey, 2008). Hands and fingers will be mapped through sensors to discover and understand the principles of animal manipulation.

This work explains a methodology for designing and construction of sensor nodes to measure forces and torques from animal or human manipulation in order to increase the spatial resolution and the precision of the measurement (Multisensorenanwendung). "Durch die Verknüpfung der Signale mehrerer Sensoren lassen sich die Zuverlässigkeit und der Anwendungsbereich vergrößern und die Signalqualität deutlich steigern. Neben einer Verbesserung der Signalqualität ergeben sich durch die Nutzung der in der Steuerung vorhanden Positions- und Richtungsinformation neue Anwendungen" (Adam, 2000). Sensor technology should be oriented to the fulfillment of the requirements of new applications in industry (Singh, 2004), and probably be based on a science oriented to market. It is our deep desire that this sensor finds a place in industrial and automotive applications (D'Ascoli, Tonarelli, & Melani, 2005).

Table of contents

1. Overview	17
1.1 Introduction	17
1.2 Significance of the research	18
2. Catalogue of Requirements	21
2.1 Overall goal	21
2.2 Main requirements of the sensor	22
2.3 Variables to be measured, the spatial force and torque in human grasping under the screw theory.	22
2.4 Environmental variables	25
2.5 Functional definition	25
3. Framework	27
3.1 General sensor concepts	27
3.2 Sensor properties	28
3.3 Environmental Parameters	33
3.4 Calibration	34
4. Sensor Model	35
4.1 Conceptual Design	35
4.2 Sensor Anatomy	36
4.3 State of the art of ring shaped force/moment sensors	37
4.4 Commercial sensors	42
4.5 Structure design	44
4.6 Elastic body for the second geometry	48
4.7 The Third geometry: an elastic body for optic solution	52
4.8 Final version	53
4.9 Environment	53

5. Design Evaluation	57
5.1 Sensitivity analysis of the strain gages position	57
6. Mathematical definition of the sensor	61
6.1 Mechanical component, structure, symmetry and material homogeneities	61
6.2 Mechanical symmetry and manufacturing	62
6.3 Material homogeneities	62
6.4 Mechanics of adhesion	62
6.5 Piezoresistive strain gauges	64
7. System and construction	67
7.1 Manufacturing of the sensor body	67
7.2 Transduction principle selection	70
7.3 Electronics	76
7.4 Communication in <i>PC</i>	80
7.5 Cabling	81
7.6 Housing	82
8. Results of the prototype and integration	83
8.1 Manufacturing and Montage of single elements	83
8.2 Manufacturing of the structure of the sensor body	83
8.3 Surface preparation	85
8.4 Strain gauges montage	86
8.5 Montage of the electronic boards	89
8.6 Assembly of the sensor	91
8.7 Visualization in Labview	91
8.8 Calibration system	92
8.9 Calibration procedure	94
9. Sensor data sheet	97

10. Discussion of critical issues	99
10.1 Understanding the energy flow	99
10.2 Simplicity	99
10.3 Knowing the variable to measure and the variables that influence the sensor performance	100
10.4 Accuracy, precision, stability and hysteresis.	100
10.5 Change of the performance in time.	101
10.6 Mechanical uncertainty and other components.	101
10.7 Piezoresistive strain gauges.	102
10.8 Adhesive fracture and cohesive fracture.	102
10.9 Hysteresis:	103
10.10 Sensor's performance:	103
11. Conclusion	105
Bibliography	107
Appendix A	115
Theses	117

Index of Figures

Fig. 1:	A pure force acting upon a three-dimensional body.	23
Fig. 2:	A pure moment acting upon a three-dimensional body	23
Fig. 3:	General case: force and moment acting on a body	24
Fig. 4:	Functional diagram of the sensor's structure	26
Fig. 5:	A model of an instrument (Helfrick, 1990).	28
Fig. 6:	Analysis of Hatamura's Geometry. (a) Mesh deformation of the sensor body by applied load in directions F_x, M_x, F_z, M_z . (b) Three dimensional mesh deformation of Hatamura's geometry under load.	38
Fig. 7:	The sensor body developed by Didden (1995)	39
Fig. 8:	Various shapes of the force sensor. (a) US Patent 4,0094,192. (b) WO 95/03527. (c) (Tsukazono, 1993).	40
Fig. 9:	A more sophisticated force sensor. (a) Force sensor from the German Aerospace Center based on optical measurement and an optical detector. (b) Force sensor from Luo (2008) based on strain gauges mounted on six beams and six joints.	41
Fig. 10:	Example of a commercial 6-axis force-moment sensor. (a) A Nano17 force sensor produced by ATI Industrial Automation. (b). Internal configuration and sensor body design.	42
Fig. 11:	Some examples of mini force sensors using various geometries and volumetric designs. (a) Kono, A (2009). (b) Viet, D.D (2008). (c) Kim, G.S (2007). (d) Lee, H. (2008).	43
Fig. 12:	Conventional cantilevers used for unidirectional deflection, (Yusuke, 2003).	44
Fig. 13:	First geometry of the sensor body that includes two double cantilever array for the axial for the transversal direction.	44
Fig. 14:	Diagram of the fully constrained double cantilever of the sensor body.	45
Fig. 15:	Diagram of the coincident double cantilever of the sensor body. (a) y-z sensor model. (b) Model of coincident beams.	45
Fig. 16:	Diagram of the coincident double cantilever applying screw theory.	46
Fig. 17:	FEA - deformation of the sensor body (first variant) under a moment load of 0.01 Nm in z-direction.	47
Fig. 18:	FEA – deformation of the sensor body (first variant) that shows transverse sensitivity under (a) Moment in direction y and (b) Moment in direction x (results of FEA).	48

Fig. 19: Mesh hexdominant of second geometry with an element sizing of 0.25 mm.	48
Fig. 20: FEA results from the single and double cantilever. (a) Equivalent strain and (b) Deformation of the cantilever.	49
Fig. 21: FEA results from the coincident cantilever: Equivalent strain. This result is important to define the position of the strain gauges.	50
Fig. 22: FEA results: Load = 0.5 Nmm, material aluminium, meshed with a solid element and constrained at four surfaces inside the ring.	50
Fig. 23: Position of the strain gauges for the measurement of and for temperature compensation.	51
Fig. 24: Final FEA results under loads (a) = 0.5 Nm. (b) = 5N.	51
Fig. 25: Design of octagonal geometry for manufacturing in glass. This design did not provide favorable results to continue working with this combination of geometry and material.	52
Fig. 26: Final version of the sensor body geometry for the hybrid concept.	53
Fig. 27: Cantilever behavior under temperature variations between 18 °C – 45 °C.	54
Fig. 28: FEA of double cantilever, increment 0.5 °C from reference temperature of 21 °C.	54
Fig. 29: ϵ_1 and ϵ_2 show symmetry in displacement under Moment .	55
Fig. 30: Temperature compensation using Wheatstone bridge.	55
Fig. 31: The sensitivity plot from demonstrates that the best position to attach the strain gauges is at 0° (A) and 180° (B).	57
Fig. 32: Sensitivity analysis of the sensor body under moment in direction x , y , z . The most important data is the maximum transverse sensitivity with a value of 10% of the maximum strain when the load M_x and M_y is applied.	58
Fig. 33: Moment of interference caused by the of the applied force when are applied direct to the sensor body.	59
Fig. 34: Sensor body modeled under ProEngineer®	67
Fig. 35: Manufacturing version of the sensor body with indication of the critical region for the mountage.	68
Fig. 36: Mechanical properties of stainless steels with different micro-structures (Kaiser Aluminum Corporation).	69
Fig. 37: Strain gauges dimensions and characteristics from the ESB models from Entran.	73

Fig. 38: Wheatstone bridge and its mathematical definition.	76
Fig. 39: Sensor configuration.	78
Fig. 40: Inside of the sensor node configuration. a) Electronic board configuration and b) board connectivity.	79
Fig. 41: The complete configuration of the Wheatstone bridges.	80
Fig. 42: <i>PC</i> Communication system of the multi node sensor system.	81
Fig. 43: Inside of the sensor design. Drawings of the sensor body and its montage.	84
Fig. 44: Prototype of the sensor body.	85
Fig. 45: Rotating and positioning system.	86
Fig. 46: Error in position of the strain gauges caused by cementation process.	87
Fig. 47: Position error during attachment of the strain gauge at the planned position.	87
Fig. 48: Integration of the full Wheatstone bridge.	88
Fig. 49: Each sensor carries 24 strain gauges. The figure compares the situation after mounting to the raw sensor body.	88
Fig. 50: Final assembly of electronic boards. Inside of the boards the microcontroller and the signal conditioners are placed.	89
Fig. 51: Final assembly of the electronic boards with dimensions about 10.5 mm x 15 mm.	90
Fig. 52: Electronic boards designed for SMD402 elements.	90
Fig. 53: Final assembly of the sensor body with 24 strain gauges.	91
Fig. 54: Visualization in Labview.	91
Fig. 55: Labview signal processing.	92
Fig. 56: Scalable design of the calibration system.	93
Fig. 57: Section through the calibration system.	93
Fig. 58: Calibration procedure assembly and diagram.	94
Fig. 59: Tools used for the calibration (a) Standardized weights used for the calibration process. (b) Standardized weights used for the calibration process. (c) Devices for reference of the moment and temperature.	95
Fig. 60: Linearity for standards weights of 10, 20, 50, 100, 200, and 500 grs. applied in direction	98
Fig. 61: Pre-strain of the gauges.	103

Index of Tables

Tab.1: Two important references for a ring-shaped force-moment sensor	39
Tab.2: Matrix of the properties of materials	69
Tab.3: (Partial) matrix of transduction principle and energy form proposed by Grandke (1989): for mechanical energy five transduction principles may be chosen.	70

1. Overview

1.1 Introduction

Sensing the forces for human grasping and motion is a complex task for understanding how human body interacts with things through manipulation (Lind & Love J, 2009) (Romero & Kjellström, 2010). Human grasping uses forces and torques to manipulate objects, changing their spatial position in many typical tasks, such as opening a door, driving a car or writing with a pen. However animals such as chimpanzees and chameleons use grasping for locomotion using their extremities as tools to realize certain actions like climbing (Laschi, Mazzolai, & Patene, 2006).

To evaluate and analyze grasping in animal and humans, it is mandatory to develop accurate mathematical models from physical ones (Hennion & Guinot, 2006). This task implies a profound exploration inside the grasping's screw to understand their effects during manipulation (Nakazawa & Uekita, 1996). In this point biomechatronics stands with its support for developing new applications inspired from the nature by increasing the performance and miniaturization of the hardware or by increasing the intelligence integrated into the system" (Dario, Carroza, & Guglielmelli, 2005). In industrial climbing machines, for example, there are quite important descriptive models of locomotion of monkeys, rats or chameleons in which each aspect of the animal's movement is clearly defined (Taylor & Chen, 2008).

A deep knowledge of human grasping and accurate biological models offer huge opportunities for building biomechatronic devices with great performance such as adaptable and ergonomic grips used in cars, motorcycles or trains need (Le, Kamm, & Kara, 2010) (Shimizu & Shimojo, 1996). This supportive knowledge (the accurate models) can be extracted by experimentation directly with animals and humans, collecting manipulation data of forces applied by the hands and fingers (Edsinger & Kemp, 2006). Because of the importance of exploring grasping forces, this work presents the design and construction of a module force sensor for the analysis of human and animal grasping. This dissertation explains the design and construction of sensor nodes (Mon & Lee, 2008) to collect data in rows of sensors to increase the spatial resolution and precision via higher object selectivity (Multisensorenanwendung). "Durch die Verknüpfung der Signale mehrerer Sensoren lassen sich die Zuverlässigkeit und der Anwendungsbereich vergrößern und die Signalqualität deutlich steigern.

Neben einer Verbesserung der Signalqualität ergeben sich durch die Nutzung der in der Steuerung vorhandenen Positions- und Richtungsinformation neue Anwendungen“ (Adam, 2000). With accurate force information, a higher possible number of sensors could be deployed in many different applications. This configuration makes it possible to have data in spatial resolutions that are difficult or impossible to obtain otherwise (Gopel, Hesse, and Zemel, 2001). According to Kumar (2004), higher spatial resolution may be achieved through the deployment of an increased number of sensor nodes. A swarm intelligence of inexpensive nodes could have higher robustness than few sophisticated and high quality sensors (Veeramachaneni & Osadciw, 2008).

Additionally, the design and construction of a sensor must include compensation mechanisms in order to compensate temperature errors and a robust signal conditioning for the environmental conditions. Some effects from the environment are likely the most important sources of errors in sensors (Wilson, 2001). A sensor cannot produce accurate measurements if environmental effects are ignored.

1.2 Significance of the research

This approach could resolve the gap between planar measuring by force plates (ground reaction force sensors) and available non-planar force-measuring devices with very restricted geometries (miniature sensors) (Liang & Zhang, 2009) (Jae & Senanayake, 2009). The integration of wireless technology and small integrated electronics with microcontroller capabilities offers new technological possibilities formerly not available.

Work performed

It was designed a 6-dimensional force sensor for grasping and ergonomics research with a linearity of 90%. This sensor was based on a miniature aluminum cylinder body with 15 mm of diameter and 14 mm of length and 28 piezoresistive strain gauges and two temperature compensation mechanisms. The design is prepared for adaptive self-configuration to work inside of a multipoint network developed under i² c. The sensor has an integrated microcontroller to permit reliable reprogramming and maintenance. It possesses also wireless Bluetooth capabilities to transfer

all multipoint information to a laptop computer over a maximal distance of 6 to 10 meters. The sensor was mounted into a environmentally protected pen application.

The structure of this dissertation begins with Chapter 2, the functional diagram of our proposal and its general objectives. Chapter 3 defines the main properties of the sensor and some environmental parameters. Chapter 4 confronts the idea behind the conceptual design of the sensor body. It is also explored some previous designs with a deep analysis of finite element. Chapter 5 explains the design evaluation of the sensor body and its sensitivity analysis. Chapter 6 summarizes the mathematical definition and superposition of the whole effects inside the sensor. Chapter 7, chapter 8 and chapter 9 detail the construction, results and sensor data sheet. Chapter 10 proposes some important topics for discussion and chapter 11 exposes the conclusion of the whole dissertation.

2. Catalogue of Requirements

2.1 Overall goal

This dissertation pursues the following goals:

Objective 1.

- a. Create a sensor to be applied for human grasping research to explore and describe grasping forces and moments. This knowledge could be fundamental to develop accurate technical devices such as ergonomic levers and bottoms and automotive devices.
- b. Develop a sensor to serve as miniature node to measure grasping forces in directions $\langle x,y,z \rangle$ and torques in directions $\langle x,y,z \rangle$ with a margin error less than 10 %.
- c. Integrate a wireless communication system to transfer the data from each node to the processing unit.

Objective 2.

- a. Explore two principles of measurement: strain gauges and optical solutions (hybrid sensor body).
- b. Explore a high spatial resolution sensing mode over the sensor surface using small transducers
- c. Explore a sensor with high strain sensitivity.
- d. Explore a sensor geometry that exhibits a low transverse sensitivity.
- e. Pursue low distortion by environmental conditions, especially temperature.
- f. Pursue simplicity in the calibration system.

2.2 Main requirements of the sensor

More precise requirements need to be defined based on two important aspects, a detailed description of variables to be measured and a detailed description of the environment represented by undesirable variables. These variables such as temperature, vibration and chemical conditions could deviate the sensor's performance, its accuracy and precision.

2.3 Variables to be measured, the spatial force and torque in human grasping under the screw theory.

Some methods like the screw theory describe the transmission of forces of a body in three dimensions. We use this tool to achieve a better understanding of the variables to be measured.

Definition 1. A Rigid body transform preserves distances and angles between vectors:

Let be $p, q \in \mathbb{R}^3$ and a map $g : \mathbb{R}^3 \times \mathbb{R}^3$ then g is a rigid body transform if

$$g_*(v \times w) = g_*(v) \times g_*(w) \quad \text{Eq. 2.1}$$

$$\|g(q) - g(p)\| = \|q - p\| \quad \text{Eq. 2.2}$$

Definition 2. A wrench is generalized force acting at a point with linear (force) elements and angular (torque) components .

$$F = \begin{pmatrix} f \\ \tau \end{pmatrix} \quad \text{where} \quad \begin{matrix} f \in \mathbb{R}^3 \\ \tau \in \mathbb{R}^3 \end{matrix} \quad \text{Eq. 2.3}$$

With this notation it is possible to find three cases represented by the following figures: a pure force acting upon a body (Fig. 1), a pure moment (Fig. 2) and a general case (Fig. 3).

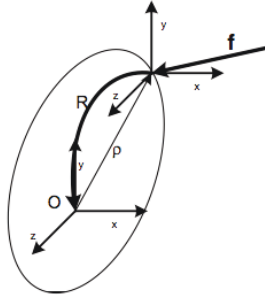


Fig. 1: A pure force acting upon a three-dimensional body.

$$W = \begin{pmatrix} f \\ 0 \end{pmatrix} \quad \text{Eq. 2.4}$$

$$W = \begin{pmatrix} f_0 \\ \tau \end{pmatrix} = \begin{pmatrix} R^T f_0 \\ R^T (-\rho \times f_0) \end{pmatrix} \quad \text{Eq. 2.5}$$

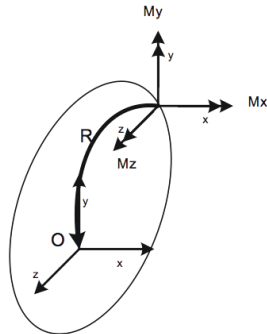


Fig. 2: A pure moment acting upon a three-dimensional body

$$W = \begin{pmatrix} 0 \\ \tau \end{pmatrix} = \begin{pmatrix} 0 \\ R^T \tau \end{pmatrix} \quad \text{Eq. 2.6}$$

$$W = \begin{pmatrix} f \\ 0 \end{pmatrix} \quad \text{Eq. 2.7}$$

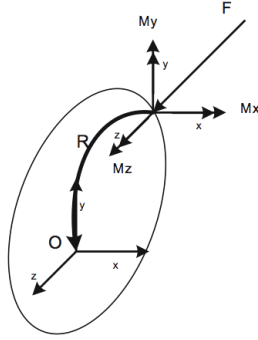


Fig. 3: General case: force and moment acting on a body

$$W = \begin{pmatrix} f \\ \tau \end{pmatrix} = \begin{pmatrix} f \\ 0 \end{pmatrix} + \begin{pmatrix} 0 \\ \tau \end{pmatrix} \quad \text{Eq. 2.8}$$

$$W = \begin{pmatrix} f_0 \\ \tau \end{pmatrix} = \begin{pmatrix} R^T f \\ R^T (-\rho \times f_0) + R^T \tau \end{pmatrix} \quad \text{Eq. 2.9}$$

$$W = \begin{pmatrix} R^T & 0 \\ -R^T \rho & R^T \end{pmatrix} \begin{pmatrix} f \\ \tau \end{pmatrix} \quad \text{Eq. 2.10}$$

$$F_T = \begin{pmatrix} f \\ \tau \end{pmatrix} \quad \text{Eq. 2.11}$$

2.3.1 The grasping map

A grasp map is composed by the configurations of k contact points that determine a net effect of the wrench applied. This could be expressed as follows:

$$W = \sum_k A^T F_T \quad \text{Eq. 2.12}$$

For multifinger grasp it is considered this wrench transformation as a formula to define a net wrench W with n contacts at frame A.

2.4 Environmental variables

The environmental parameters will be understood as external variables such as temperature, humidity, and vibration. These variables affect the performance of the transducer if any consideration is made about the material, geometry, electronic compensation or the conceptual design of the sensor. Each environmental parameter is measured indirectly or affects in some way the components of the sensor. For example, a temperature variation for human or animal contact (Sen, Das, & Zhou, 2007) could produce geometric variations in metallic components or could produce a different electromotive force between two points (thermoelectric effect) at resistance or piezoresistive gauges. Every undesirable variable reflects its influence on the sensor output, producing static or dynamic variations affecting directly the linearity, precision and accuracy. This dissertation considers temperature as the most important environmental parameter.

2.5 Functional definition

To avoid vague specifications the sensor must be able to do the following:

- a. Trace 6-dimensional grasp forces from human grasping with the construction of a sensor able to perform a non-planar measurement with a non-linearity equal or less than 10%.
- b. Communication interface with an end user, such as a laptop, through a wireless interface.
- c. Having a free maintenance sensor.
- d. Having a scalable operating system.
- e. Having an environmentally protected and durable housing for grasping experimentation.

More specific functional definitions are in shown in Figure 4.

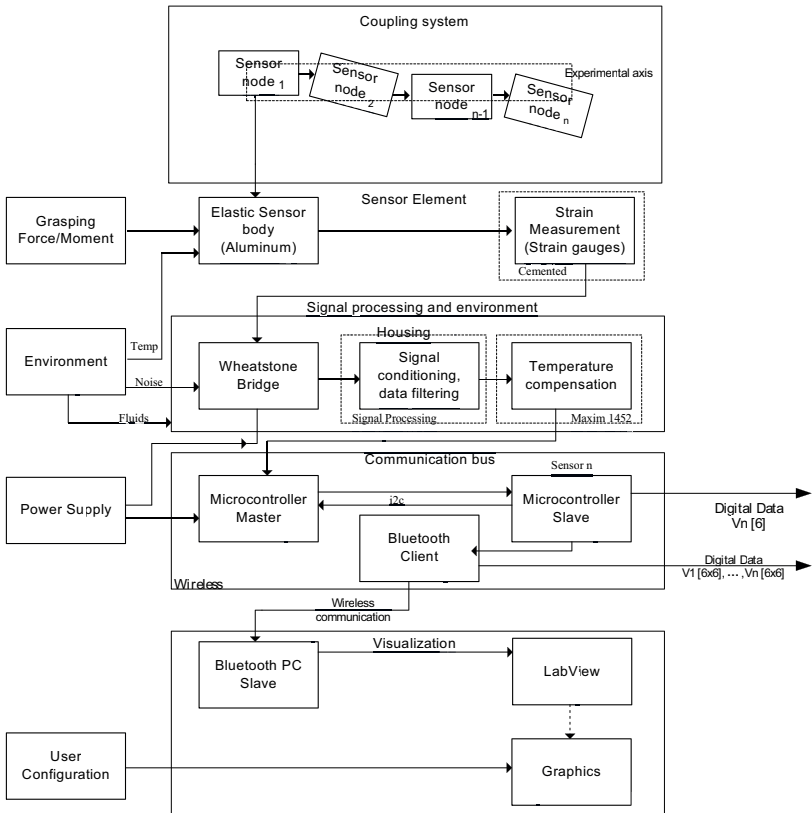


Fig. 4: Functional diagram of the sensor's structure

Summarizing, sensors are most commonly used to make quantifiable measurements, as opposed to qualitative detection (Wilson, 2005) (Jae, Senanayake, & Gouwanda, 2009). Therefore the requirements of the measurement will determine the selection and applications of the sensor (Fang & David, 2006) (Kuwahara & Kawaji, 2006). The environment conditions are perhaps the most important contributor to measurement errors in the measurement systems (Wilson, 2005). This issue must be considered as an important design requirement to reach the accuracy and reduce the uncertainty of the measurement.

3. Framework

3.1 General sensor concepts

Sensors convert physical variables to signal variables (Kanoun & Trankler, 2004) through different components, such as sensor body, transducer principle and signal conditioning. Sensors are often defined as transducers that transform input energy into an electric signal. Juckenack (1990) defines sensor as sensor body or transducer (Fühler). This concept connects physical variables such as force or temperature to a response of a particular physical effect like piezoresistance or optical resistance. Tränkler (1998) interprets the term sensor as a system involving three parts: a) sensor body converting energy into electric form; b) signal conditioning; and c) signal processing elements. Tränkler (1998) gives the name of sensor element to an energy converter that transforms physical, chemical or biological phenomena into electric signals. Grandke (1989) exposes a difference between a sensor and a transducer, which only translates one type of energy to another.

On the other hand, sensors are used to gain quantitative data. Many kinds of mechanical sensors are built to measure mechanical quantities such as force, torque, power, stress, displacement, rotation, strain, acceleration and pressure, applying different types of technologies. Depending on its basic principle, the sensor estimates quantities by a “side effect” that reveals some degree of variation of other physical variables, for example temperature. The ISO standard DIN-ISO 1319-3 defines estimate “as estimation or value close enough to the variable that is measured”. For example some force sensors doesn’t measure the force directly but rather the effect produced by the load applied (strain or deformation).

Webster (1998) defines sensors as nodes from a more complicated measurement net. On the other side Taylor (1997) defines Measurement as a comparing process of an unknown quantity with a standard of the same quantity. Webster (1998) classifies the sensor from an energetic point of view. This classification describes active and passive sensors. Active sensors are defined as elements that require an external source of excitation to work. On the other hand, passive sensors generate an electrical signal without any external energy support. One example of this category is a contact sensor of Polyvinylidene fluoride (PVDF).

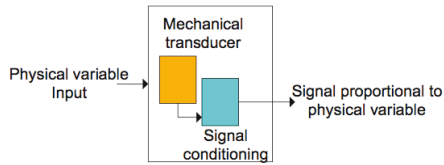


Fig. 5: A model of an instrument (Helfrick, 1990).

Figure 5 presents a generalized model of a simple sensor. The physical variable is converted into an electrical signal variable (output) that can be manipulated or transformed. It is possible to display, record, or use the electrical signal as an input to some secondary device system (Helfrick, 1990). This signal can be used by a system of which the instrument is a part, for controlling or monitoring operations. If the signal output has a very small magnitude, it will be necessary to amplify the output. The amplified output may be digitized and transmitted, for example by wireless bus, or simply displayed by a measurement software.

Besides measurements, appear undesirable (physical) variables, such as environmental temperature or mechanical vibration. These variables could cause an influence defined as measurement deviation or Messabweichungen by DIN 1319-3.

3.2 Sensor properties

3.2.1 Accuracy and error

According to Webster (1998), “the accuracy of an instrument is defined as the difference between the real value and the value of the measurement”. It is expressed as percent of full scale. DIN 1319-3 defines uncertainty of measurement (Messunsicherheit) as the uncertainty of a quantity because of accuracy and a characteristic of the dispersion of the measurement. This uncertainty is responsible for the difference between the true and the measured value.

On the other hand, errors in experimental measurements can be categorized as either random or systematic (Grandke, 1989). Random errors will cause scatter deviations of results from the true value. With an increasing of the number of measurements,

the average value will approach the true value. Systematic errors, on the other hand, generate a positive or negative bias (Juckenack, 1990). Every measurement will contain some error due to systematic (bias) and some to random or noise error sources (Grandke, 1989). A variety of factors can contribute in systematic errors. If the source of the systematic error is known it can be corrected by compensation (Tränkler, 1998). There are other factors that also cause a change in sensor calibration, resulting in systematic errors. For example, the aging of the components could change the sensor response and hence its calibration. *“Calibration of the sensor can change by damage or over limited use. For this reasons the sensor should be recalibrated periodically”* (Grandke, 1989).

In spite that systematic errors can be removed, some random error will remain carrying no useful information (Juckenack, 1990). It is called random error and it is referred as noise. If a measurement with true random error is repeated a large number of times, it will exhibit a Gaussian distribution, centered on the true value (assuming there is no systematic errors). So the average of all the measurements will yield a good estimate of the true value (Juckenack, 1990).

There are a variety of sources of randomness that degrade the precision of the measurement and its repeatability. For example, the planarity measurement of a rough surface will depend on the exact location.

The most important static and dynamic characteristics of a sensor are explained by (D’Amico & Di Natale, 2001) Grandke (1989), Wilson (2005) and Tränkler (1998).

3.2.2 Static characteristics

1. *Accuracy*: A measure of how closely the result of the measurement (sensor output) approximates the true value. DIN 1319-3 defines inaccuracy as follows:

$$u(x_i) = s(\bar{v}) = \frac{s}{\sqrt{n}} = \sqrt{\frac{1}{n(n-1)} \sum_{j=1}^n (v_j - \bar{v})^2} \quad \text{Eq. 3.1}$$

Inaccuracy is expressed as a percentage of full-scale output (FSO).

2. *Precision*: Describes how disperse is a measurement and it is not related with how accurately is the measurement.

3. *Resolution*: It is the smallest increment of the measurand that produces a detectable increment in the output. It is expressed as a percentage of the measurand range (% MR).

4. *Sensitivity*: Incremental ratio of the output to the input variable that the sensor has to measure.

5. *Selectivity*: In non-ideal sensors, the output might change owing to a change in the environmental parameters or other variables. Selectivity S is expressed as ratio of output signal and the disturbing variable:

$$S = \frac{\text{output signal}}{\text{disturbing variable}} \quad \text{Eq. 3.2}$$

An ideally non-selective sensor is designated to have a selectivity of $S = 0$.

6. *Minimum detectable signal (MDS)*: Assuming that the signal does not contain any noise, the minimum signal level that yields a readable transducer output is determined by the noise performance of the transducer. To account for the noise level generated by the transducer, all the internal noise source of the transducer can be accumulated together to form a single noise source. This single noise source, which is called the equivalent input noise source, when is connected to the input of the ideal (noiseless) transducer, yields the output noise level of the transducer under study. The minimum signal level that yields a reliable transducer output signal, the MDS, is usually taken as the root-mean square (RMS) equivalent input noise (signal-to-noise ratio of 0 dB).

7. *Threshold*: Starting from a measurand of value zero, the smallest initial increment in the measurand that results in a detectable output is the threshold. Threshold is usually due to device nonlinearity and is different from MDS.

8. *Nonlinearity*. A measure of deviation from linearity is defined by $y_1 = f(x_1)$ and $y_2 = f(x_2)$ then $y_1 + y_2 = f(x_1 + x_2)$ of the sensor, which is usually described in terms of percentage deviation in full scale output at a given value of the measurand. There are two methods to specify non-linearity: a) deviation from best-fit straight line and b) deviation from terminal-based straight line. The first method expresses the deviation of the transducer output from a best-fit straight line. The second method expresses the

deviation of the output from a straight line that is drawn between the two terminal ends of the output versus input curve.

9. *Deviation from an expected output*: In some cases distortion is a measure of deviation from linearity. However, in general it need not be related to nonlinearity at all. For example, the distortion at the output of an electronic sinusoidal oscillator, which is inherently a non-linear device, is a measure of the deviation of the output from an ideal sinusoidal waveform. In the case of an amplifier, the distortion at the output is caused by non-linearities that result in the presence of frequency components at the output but they are not present at the input.

10. *Conformity*: Closeness of an experimental curve to a theoretical curve or to a curve obtained using least-squares or other fits. It is expressed in % FSO at any given value of the measurand.

11. *Hysteresis*: Difference in the output of the sensor for a given input value X when X comes from two opposite directions, i.e. x^+ , x^- . Hysteresis in mechanical sensors is usually caused by a lag in the action of the sensing element. There are two other causes that may result in hysteresis-type behavior, and they are not considered as true hysteresis (Grandke 1989). These are friction error, which is usually observed in potentiometric transducers, and backlash error, which is usually observed in mechanical actuators that employ gears.

12. *Repeatability*: The difference in the output readings at a given value of the measurand X , where X is consecutively measured.

13. *Span (Operating range, full scale range)*: The range of input variable that produces a meaningful sensor output.

14. *Noise*. Random fluctuation in the value of the measurand that causes random fluctuation in the output. Noise at the sensor output is due to either internal noise sources, such as resistors at finite temperatures, or externally generated mechanical and electromagnetic fluctuations. AC power line interference (50 Hz or 60 Hz) and other external interferences are also considered as noise, when they are not random. The external noise will become more important as the transducer size is made progressively smaller. The external noise in a sensor is primarily associated with the random fluctuations of the particular measurand, which usually has several different

components. Most of the components can be identified as the equivalent of one of four types of internal noise mechanisms, which are usually electrical in nature: shot noise, Johnson (or thermal) noise, recombination-generation (r-g) noise and flicker noise. Shot noise is caused by charge carriers crossing a barrier at random. It is present in Schottky barrier diodes, p-n junctions and the thermionic emission. Johnson noise is provoked by random motion of charge carriers which produce a fluctuating electromagnetic force at the output terminal. It is present in all resistive components. R-g noise in semiconductors is caused by trapping and detrapping of charge carriers, causing a random fluctuation in the number of carriers and resistance. Among commonly encountered r-g noise is burst noise. Flicker noise has a spectral density that varies inversely with the frequency, being very large at very low frequencies. "The origin of flicker noise is not yet well understood and recent experimental results suggesting fluctuation in the carrier mobility are still inconclusive" (Wilson 2005). In practice the noise generated at the transducer is usually not a limiting factor of the measurement accuracy (Wilson 2005).

15. *Output impedance*: This is the transducer output impedance that offers the sensor to the following amplifier stage.

16. *Grounding*: This is performed to establish a common node among different parts of the system with the requirement that no potential variation along this common node with any point inside the node may occur.

17. *Isolation*: This is performed to reduce undesirable electrical, magnetic, electromagnetic, and mechanical coupling among parts of the system and between the system and the outside environment.

18. *Instability and drift*: Change of sensitivity or the output level (with zero input) with time, temperature, and any other parameter that is not considered part of the input.

19. *Overall Performance*: The overall performance is determined by the geometric sum of the performance errors adding all of them in the same time.

3.2.3 Dynamic Characteristics

20. *Transfer Function:* $H(s) = \frac{Y(s)}{X(s)}$ expresses the relation between the output and the input expressed in terms of Laplace transformation.

21. *Frequency response.* Change of the phase and amplitude of the output as a function of the frequency of a unit amplitude sinusoidal input. It is displayed graphically as plots of $10 \log |H(\omega)|$ and phase of $H(\omega)$ versus $\log(\omega)$, where $H(\omega)$ is the Fourier transform of the impulse response described below. These plots are called Bode plots.

22. *Impulse response.* $h(t)$ is the response of the system to a unit impulse of the stimulus. The Fourier transforms of $h(t)$ gives the frequency response of the system.

23. *Step response:* The response of a transducer to a step change in the input. It is usually described in terms of rise time, decay time, and a time constant.

3.3 Environmental Parameters

The effect of temperature on a sensor is determined by two components that are expressed as % FSO: temperature zero error and temperature span error. Potter (2000) defines the temperature zero error as the change in the output level of a transducer with respect to variation of temperature when the measurand is set to zero. On the other hand, temperature span error is the change in the output level of a transducer due to temperature variation when the input (the measurand) is set equal to its full scale (100% MR). Temperature performance is usually expressed by an error bar for given values of measurand and temperature. Putting these error bars next to each other, at different temperatures the butterfly specification can be obtained (Potter, 2000). Using the butterfly specification, the upper and lower bounds of the transducer output are determined at any given temperature.

3.4 Calibration

It is the procedure of the closeness from the measurement to the real value through a device or a known measurement patron. Grandke (1989) defines calibration as the relationship between the physical measurement variable (input) and the signal variable (output) for a specific sensor. Typically a sensor (or an entire instrument system) is calibrated measuring the response provided by known physical standard to the system.

4. Sensor Model

4.1 Conceptual Design

Essentially the functions of a sensor as an elastic body follow the general dynamical equation $M(\ddot{q}) + V(q, \dot{q}) + K(q) + G(q) = \tau$. With this model the sensor uses a special geometry to concentrate the mechanical force to the elastic component. Under ideal conditions the energy transfer is linear for the elastic equilibrium. This local strain is converted into a useful signal by the transducer. A transducer, i.e., a piezoresistive strain gauge, changes its nominal resistance under mechanical stress. This piezo characteristic is very useful for force measurement when strain gauges are bounded at the surface of a deformable body. With a growing demand of punctual sensors in specific applications, sensor becomes more and more desirable with special characteristics and functions, for example, connectivity to wireless networks (Brasche, 2008). Therefore the uses of reliable and adequate modeling tools are more important than ever. (Granke & Thomas, 1989).

To reach the objectives of the sensor various types of operation were analyzed, but the design was focused on two transducer methods, the first strain measurement through cemented strain gauges, and the second strain measurement using opto-elasticity reflective material or glass body. First choice was the cemented strain gauges because of its simplicity and available technology. This model serves as valuable heuristic tools for the design of a trial device. Making the choice of appropriate operation model, physical and material parameters could determine the precision of the sensor operation. Typically the measurement of force with strain gauges uses the deformation of a body to its elastic deformation limit. Design needs an analysis interaction between mathematical and finite element to find the best geometric solution. Every possible solution must to resolve the most important criteria, the *transverse-sensitivity*. This term is defined as the transverse effect produced in the output of a sensor that is caused by a load which is not primary related with the axis that the sensor intends to measure. Vishay (2006) defines these terms as behavior of the gauge resulting from strains which are perpendicular to the primary sensing (axis) of the gauge. Elimination of the transverse-sensitivity could enhance the overall performance and it could simplify the post-processing operation, calibration and multivariate data analysis.

This work used a heuristic method for the design process. This method combines interactions of Finite Element Analysis (FEA) with mathematical models and sensitivity analysis. These three components play an important role to discover the optimal performance of the sensor body. This task implies an isolation of deformation in a very small area of sensor's surface in relation to manufacturing and geometry complexity. This process could reduce significantly the transverse-sensitivity.

Because of mechanical coupling of the sensor body there is no way to remark totally the strain into specific points, or find a totally isolation for the deformation as cause of just one uni-directional force or torque any part of the body, but any intent in geometry design could improve the partial transverse-sensitivity. One option could be a very simple geometry such as a cylinder. Positioning transducers at different points on the surface could produce enough information about the mechanical performance of the body. This design translates the success of the sensor to a signal post-processing or to a multivariate analysis in order to find a linear relation with the external loads.

The conceptual design of the sensor is expressed in figure 4. It integrates the following components: a) coupling system; b) sensor element; c) signal processing and environment; d) communication and e) visualization.

4.2 Sensor Anatomy

4.2.1 Coupling system

The coupling system is part of a multipoint measurement system where each sensor node constructs the experimental axis. A sensor alone would not be adequate to support this application, but in conjunction they could enhance their capabilities (adding effect). Peter H. Veltink (2005) concludes that deploying low cost sensors in larger number is more effective than deploying high-end sensors. Instead of choosing a group of faster and expensive sensors this dissertation introduces a design of smaller and limited sensor, to be deployed in larger number, improving the density of measurements, maintenance and flexibility.

4.2.2 Sensor body design

A sensor body is the heart of the sensor, the mechanical effectiveness of the design and the integration with the transducer marks a fingerprint on its performance. On the other hand, the goal of numerical modeling is to understand the sensor's operating principle, in particular way, how the design, fabrication, and operating parameters determine, enhance or limit its properties such as accuracy (Swiss Federal Institute of Technology ETH 2005)). A key task to perform a precise deformation distribution is the establishment of clear rules for the design of the geometry. These rules could limit the transverse-sensitivity and could improve the understanding of the interaction between loads (wrenches) and the body. A complex surface design could reduce the transverse-sensitivity, but it could increase the complexity of manufacturing. On the other hand a simple surface design reduces the manufacturing complexity but increases the transverse interference and obviously increases the complexity of calibration. Therefore a compromise is needed to find the best solution between interference, manufacturing and calibration complexity.

4.3 State of the art of ring shaped force/moment sensors

This work will concentrate in two questions about the force-moment sensors (based on elastic bodies). First, it is possible to reduce considerably the transverse-sensitivity acting on the sensor body and how do previous works have resolved it.

4.3.1 Hatamura's geometry

Figure 6 shows the deformation of the ring-shaped 6-axis sensor described in Hatamura (1989). This geometry reduces the ratio of the rated moment with respect to the rated load eliminating the second component of the torque produced by the radius of the ring (ρ) as is shown in figure 4-2. This improvement reduces the transverse-sensitivity and enhances the accuracy of the sensor.

Instead of some of previous developments, which develops with planar structures of different geometries, Hatamura introduced a 6 axis torque-force sensor with a ring form.

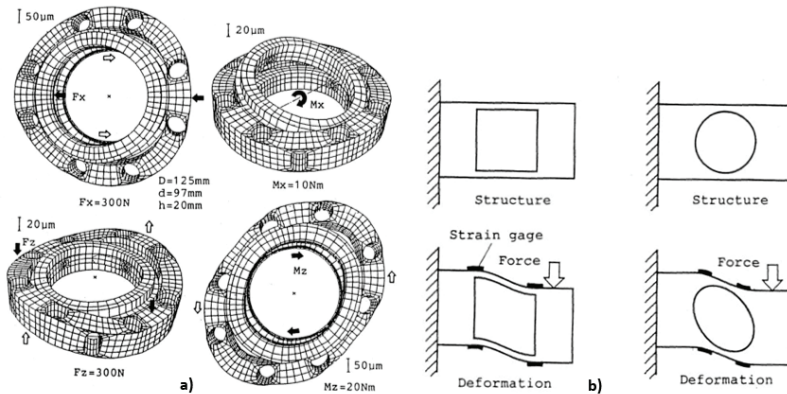


Fig. 6: Analysis of Hatamura's Geometry. (a) Mesh deformation of the sensor body by applied load in in directions F_x , M_x , F_z , M_z . (b) Three dimensional mesh deformation of Hatamura's geometry under load.

The sensor uses a parallel plate construction with eight axial holes and four radial holes. It applies 28-cemented strain gauges with 7 full Wheatstone bridges. The strain gauges positions were defined by Finite Element results.

The sensor body has a ring form with 8 small holes where is identified the deformation distribution. On the other hand, this sensor improves a concentric tool to approach the end effector increasing the sensitivity of the sensor, and avoiding the disturbance of the inertial forces. Also this parallel structure brings high sensitivity, low transverse sensitivity, high rigidity, stability, and linearity. Because of its large hole in the center of its geometry it is possible to install any kind of tool. The most important contribution of this work is the reduction of the ratio of the rated moment to the rated load, which improves considerably the accuracy of the sensor and reduces the transverse sensitivity.

4.3.2 Didden's Geometry

Figure 7 shows a ring-shaped three-axis micro force/torque sensor, developed by Didden (1995). This works describes the design of a ring shape based on Hatamura (1989). It defines eight holes shaped geometry in order to localize the strain on the

planar face of the ring. The most important contribution is the development of small strength geometrics over a three dimensional surface.

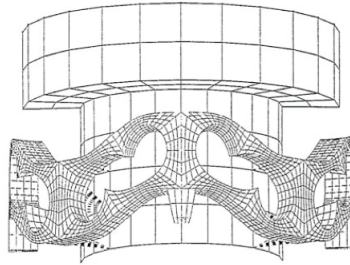


Fig. 7: The sensor body developed by Didden (1995)

Tab.1: Two important references for a ring-shaped force-moment sensor

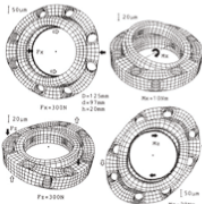
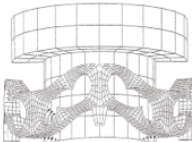
Concept	Contributions	
<p>1. Hatamura Geometry</p> 	<p>Deformation of the ring-shaped 6-axis sensor</p> <p>The sensor body is composed of a ring with 8 small holes between of them identify the best possible</p> <p>It introduces a ring shape to reduce the distance from the tools improving a concentric tool axis, increasing the sensitivity of the sensor, avoiding the disturbance of the inertial forces from the end effector.</p>	<p>1. Brings high sensitivity, low transverse sensitivity, and high rigidity.</p> <p>2. Reduction of the ratio of the rated moment to the rated load.</p>
<p>2. Didden's Geometry</p> 	<p>Ring-shaped three-axis micro force/torque sensor is introduced, developed by the Catholic University of Leuven .</p>	<p>1. A force-moment sensor under geometrical restriction,</p>

Table 1 compares the main contributions of the two most important geometries of the force torque sensor (Hatamura, 1989 and Didden, 1995)

4.3.3 Others geometries

Figure 8 shows different configurations of deformable elements. Figure 8 (a) is a small ring with a three side structure inside. This sensor uses the inner side to attach the strain gauges. There is no information about the performance of the sensor.

Figure 8 (b) the sensor body is a force sensor converter using resilient connection members (2, 4, 6) that extend to a central hub. This sensor uses a quite simple form that improves simplicity to mount the strain gauges. In figure 8 (c) is shown a multi arm sensor body for detecting the force and moment components of the force acted on an industrial robot arm.

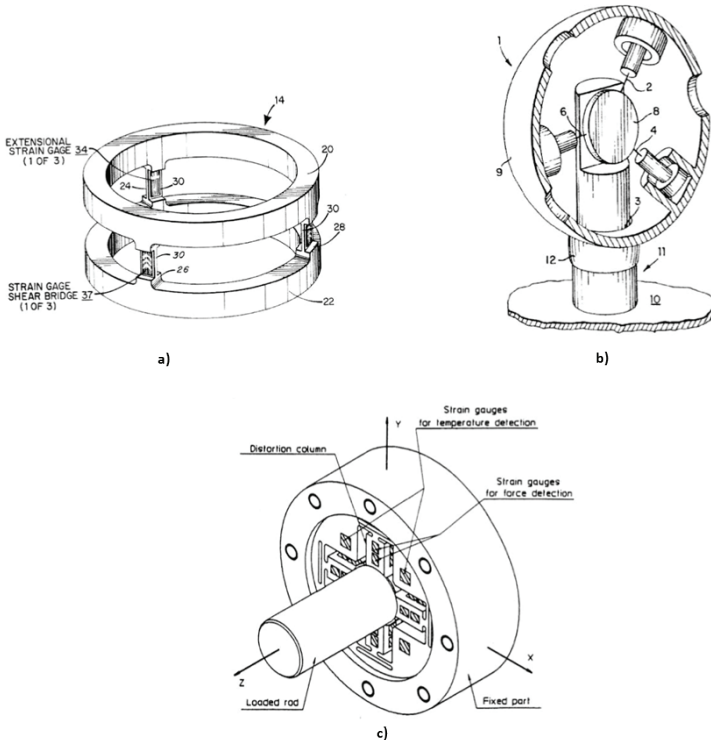


Fig. 8: Various shapes of the force sensor. (a) US Patent 4,0094,192. (b) WO 95/03527. (c) (Tsukazono, 1993).

Figure 9 (German Aerospace Center, 2004), Luo (2008), show a more sophisticated force sensor. Figure 9 (a) is based on optical measurement where each deformation produces a change in the energy received by the optical detector. This kind of sensor demonstrates a very high sensitivity. Figure 9 (b) Luo (2008) is a force sensor based on six beams and six joints composed with six triangles with equal angles in same size.

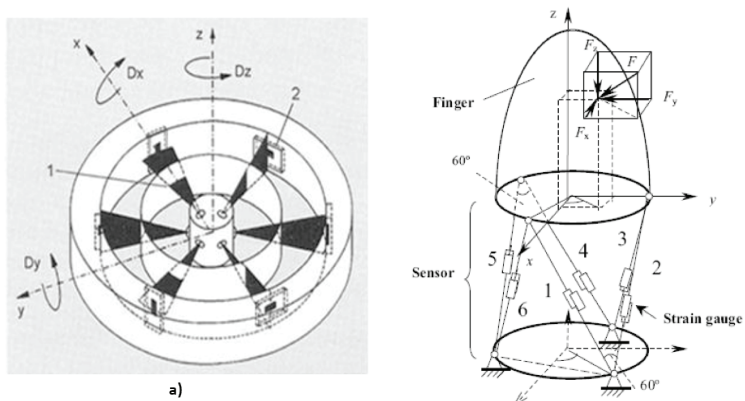


Fig. 9: A more sophisticated force sensor. (a) Force sensor from the German Aerospace Center based on optical measurement and an optical detector. (b) Force sensor from Luo (2008) based on strain gauges mounted on six beams and six joints.

4.4 Commercial sensors

On the other hand there is a commercial product available, Nano17 from ATI Industrial Automation shown in figure 10. This sensor introduces an overload protection and uses strain gauges to extract the deformation of the surface from the four beams sensor body. Its commercial value is about 5,000 €.

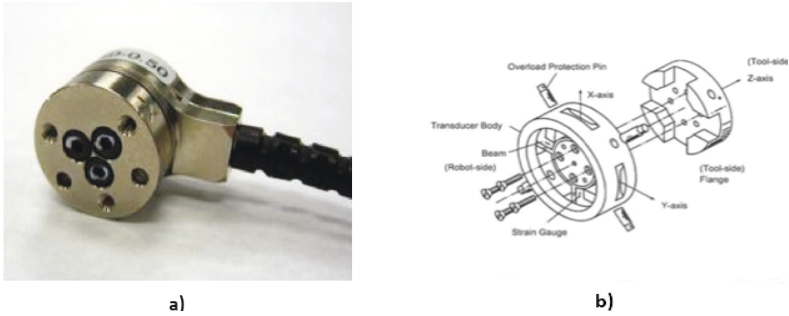
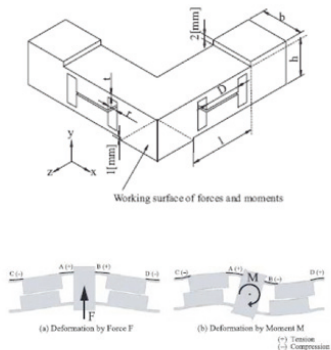


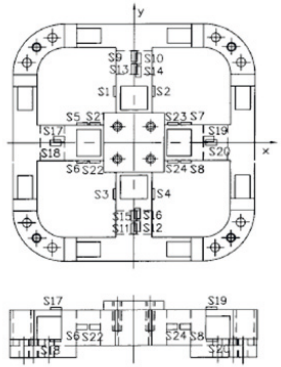
Fig. 10: Example of a commercial 6-axis force-moment sensor. (a) A Nano17 force sensor produced by ATI Industrial Automation. (b). Internal configuration and sensor body design.

The sensors bodies shown in 11(a), 11(b), 11(c) y 11(d) have different geometry but they aim to the same objective, obtain the best-localized strain regions with a minimum transverse sensitivity in axes x , y , z under the loads F_x , F_y , F_z , M_x , M_y , M_z .



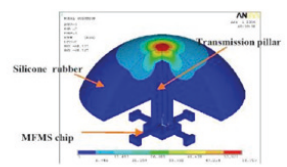
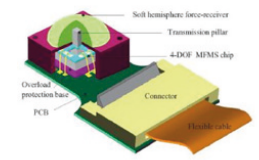
Kono, A(2009)

a)



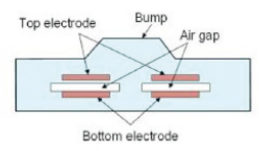
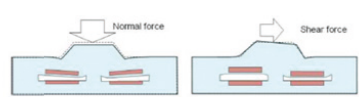
Kim, G.S(2007)

c)



Viet, D.D (2008)

b)



Lee, H.(2008)

d)

Fig. 11: Some examples of mini force sensors using various geometries and volumetric designs. (a) Kono, A (2009). (b) Viet, D.D (2008). (c) Kim, G.S (2007). (d) Lee, H. (2008).

4.5 Structure design

Cantilevers are important design elements in force sensors to isolate unidirectional deflection. Some cantilevers as figure 12 have variations in form and geometry to induce a clear deflection and strain. Without a doubt cantilevers will be important elements for our sensor design.

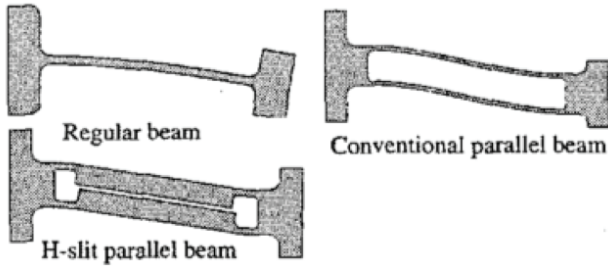


Fig. 12: Conventional cantilevers used for unidirectional deflection, (Yusuke, 2003).

4.5.1 First design

The first design is based on ring geometry and four cantilever elements, showed in figure 13. This design develops a volumetric measure of the strain on the surface of the sensor body and not just in a planar surface. The first solution includes two double cantilevers, two for the axial direction and two more for the transversal direction.

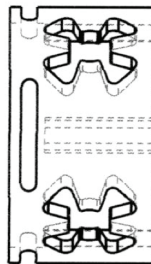


Fig. 13: First geometry of the sensor body that includes two double cantilever array for the axial for the transversal direction.

4.5.2 The double cantilever principle

The model shown in figure 14 and figure 15 represents the double cantilever principle of the sensor. The deformation in each cantilever acts in opposite direction. When one cantilever acts in tension the other cantilever acts in compression. For example, if load M_z changes its direction, the performance of the beams changes, too.

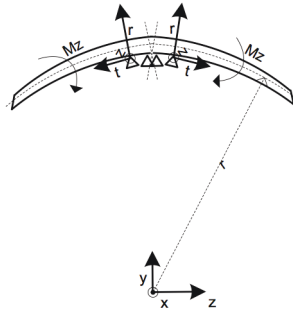


Fig. 14: Diagram of the fully constrained double cantilever of the sensor body.

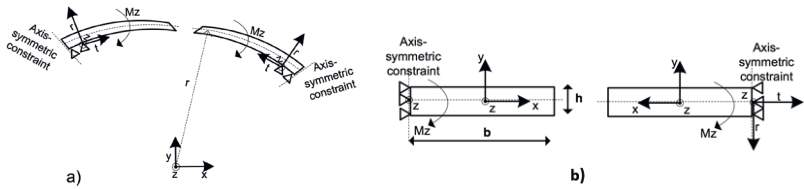


Fig. 15: Diagram of the coincident double cantilever of the sensor body. (a) y-z sensor model. (b) Model of coincident beams.

The cantilever or bending stress can be calculated with equation 15 at diverse levels of zero-stress axis.

$$\sigma_y = \frac{M_z}{I} c \quad \text{Eq. 4.1}$$

where:

M_z is the bending moment in direction z .

c is the distance from the neutral axis.

I is the second moment of area about its neutral axis.

For a rectangular beam the second moment of area can be calculated with

$$I_x = \frac{bh^3}{12} \quad \text{Eq. 4.2}$$

$$I_y = \frac{b^3h}{12} \quad \text{Eq. 4.3}$$

It is important to consider the leverage arm when a load is applied to the ring. This is one of the main reasons of transverse sensitivity.

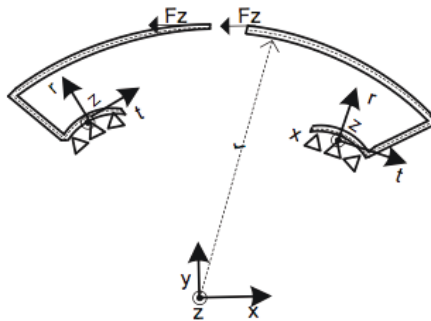


Fig. 16: Diagram of the coincident double cantilever applying screw theory.

Figure 16 shows that force $R^T f$ is a pure force f_x, f_y, f_z . This force causes an undesirable effect or moment $R^T (-\rho \times f)$. So the ratio of transverse sensitivity between f_x and M_x and between f_y and M_x has a relation to the radius ρ . On the other side the elastic body uses characteristics, such as calculated moment of inertia and symmetry to increase the sensitivity of the measurement, the location of the stress at specific zones (strain distribution) and produce an isometric performance.

4.5.3 Elastic body, first finite element analysis

The first geometry has two double cantilevers, one in axial direction and the other in transverse direction. The Finite Element Analysis in figure 17 describes the structure performance under a load of M_z . This preliminary analysis shows high sensitivity in z direction over two small regions of the surface at the axial double cantilever rejecting strain on other regions.

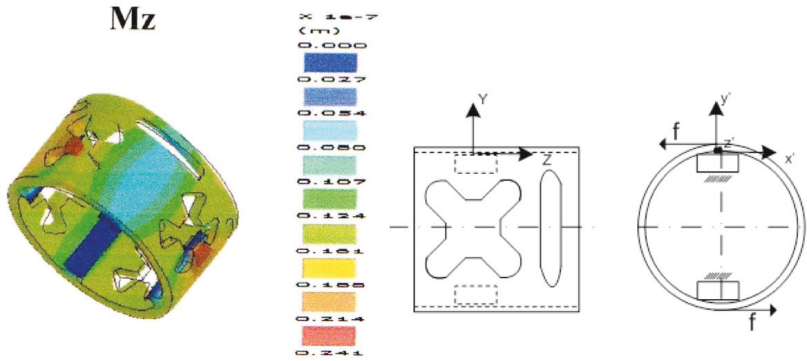


Fig. 17: FEA - deformation of the sensor body (first variant) under a moment load of 0.01 Nm in z-direction.

On the other hand the transverse sensitivity of M_x and M_y from the double axial cantilever region is approximately **10.8%**. Figure 18 shows an extreme transverse sensitivity at the end of the ring. The computed transverse sensitivity for M_x and M_y is near of **77.4 %** with a maximum stress phased 90 degrees.

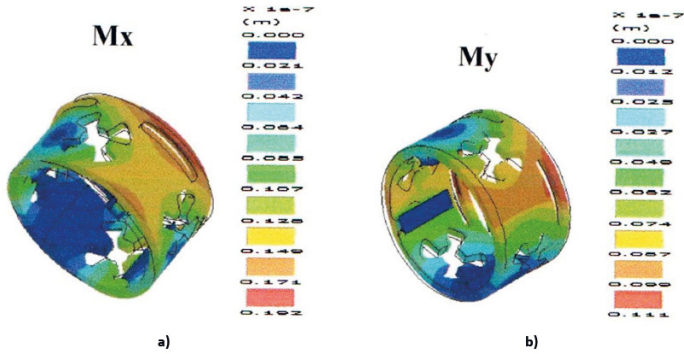


Fig. 18: FEA – deformation of the sensor body (first variant) that shows transverse sensitivity under (a) Moment in direction y and (b) Moment in direction x (results of FEA).

4.6 Elastic body for the second geometry

The first analysis showed that the sensitivity of the axial double cantilever is approximately 56% higher than the sensitivity in cross direction. This fact could raise questions about the necessity of maintaining the two transversal beams. Therefore the second design eliminates these two transversal beams and introduces eight semicircular geometries near to the cylinder edge. The second design is shown in figure 19. It is important to remark that these changes simplify the machinability of the ring.

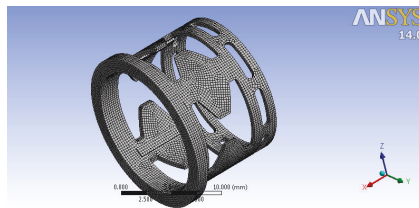
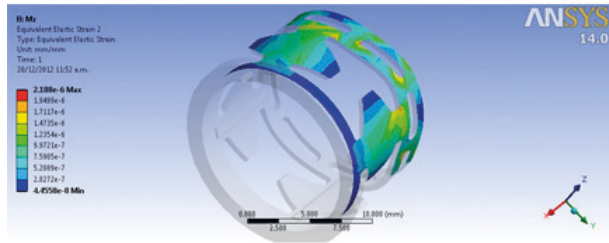


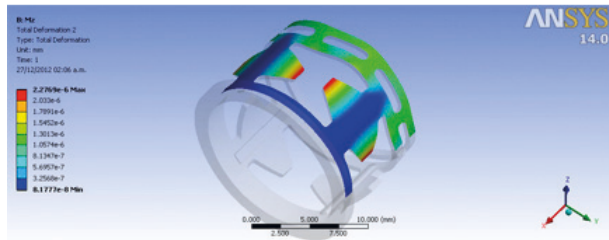
Fig. 19: Mesh hexdominant of second geometry with an element sizing of 0.25 mm.

4.6.1 Finite Element Analysis of single cantilever

The function of a single and double cantilever was modeled in Finite Element. Figure 20 shows the deformation and the strain of a single beam under a load of M_z . The maximum strain is 87.47% higher than the minimum value. This result gives enough evidence to bond strain gauges over this small region.



a)



b)

Fig. 20: FEA results from the single and double cantilever. (a) Equivalent strain and (b) Deformation of the cantilever.

Figure 21 shows strain symmetry of the coincident cantilevers, left compression and right tension.

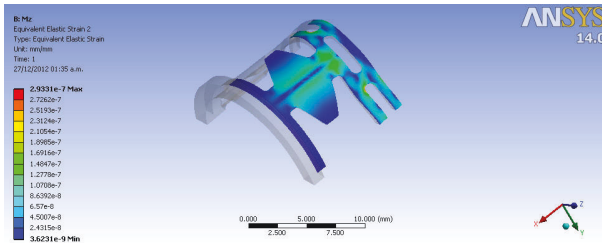


Fig. 21: FEA results from the coincident cantilever: Equivalent strain. This result is important to define the position of the strain gauges.

The result of the simulation in figure 22 confirms the high sensitivity obtained in the design of the sensor body. In fact, it could be concluded the best regions to apply four strain gauges over the two double beams. This could be translated for two in compression and two in tension. Moreover, this work proposes two more strain gauges for self-compensation of temperature at the low strain line, just at the end of the beams.

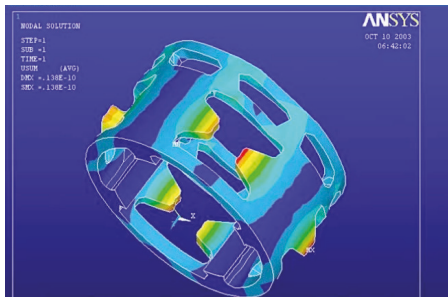


Fig. 22: FEA results: Load = 0.5 Nmm, material aluminium, meshed with a solid element and constrained at four surfaces inside the ring.

The position of each strain gauge is explained in figure 23.

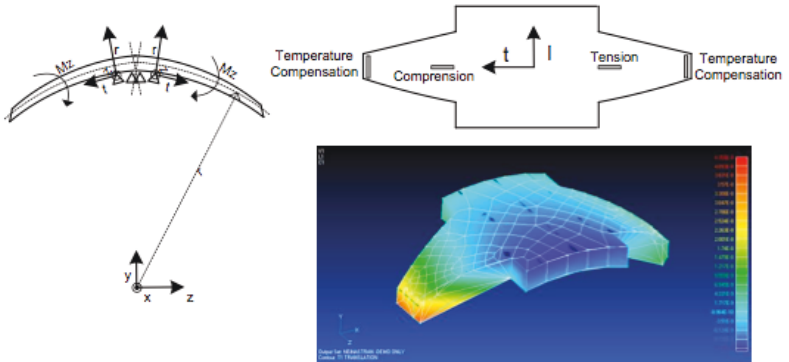


Fig. 23: Position of the strain gauges for the measurement of and for temperature compensation.

The results of FEA analyses for and are shown in figure 24. It is possible to observe a high strain region at the middle of the semicircular geometry. This region is good for positioning four strain gauges, two at the outer diameter (tension) and two at the inner diameter (compression). Moreover, figure 24 displays two highly sensitive regions for that are optimal for the positioning of four strain gauges.

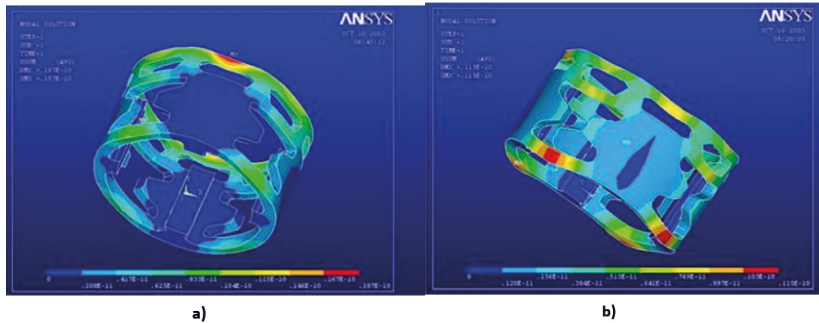


Fig. 24: Final FEA results under loads (a) = 0.5 Nm. (b) = 5N.

4.7 The Third geometry: an elastic body for optic solution

An 8-side geometry solution (figure 25) was explored as more sensitive solution based on glass. The finite element simulation shows that the effect of the double cantilever was transferred to the edge of the geometry. This design did not provide favorable results to continue working with this combination of geometry and material.

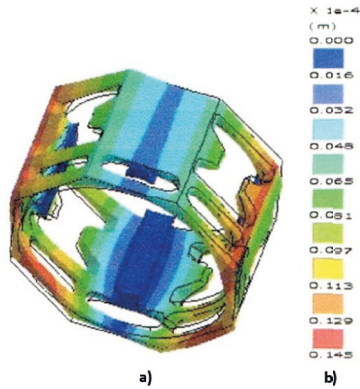


Fig. 25: Design of octagonal geometry for manufacturing in glass. This design did not provide favorable results to continue working with this combination of geometry and material.

4.8 Final version

At the ending stage of the iterative design the decision fell in the geometry shown in figure 26.

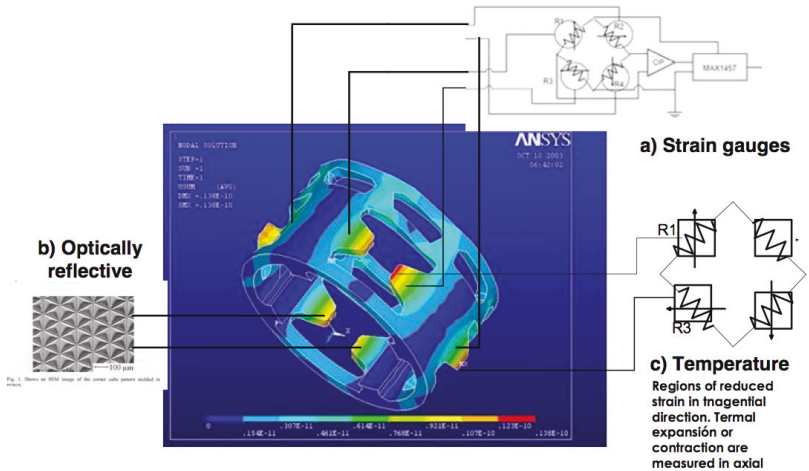


Fig. 26: Final version of the sensor body geometry for the hybrid concept.

4.9 Environment

4.9.1 Temperature compensation in the elastic body

It is important to describe the relevant physical effects inside the sensor caused by temperature. These temperature effects act as well via the mechanical behavior of the aluminum ring, via the piezoresistive transducers, and via the electronic components. With pertinent circuitry, amplification, biasing, and dynamic signal correction (compensation) can be achieved an output voltage or current proportional to absolute temperature (Göpel, 2000). This dissertation proposes two temperature compensation methods, the first integrated in the sensor body to detect small strain changes in the aluminum ring (attached at the edge of the double cantilever), and the second with an external electronic component such as the MAX1457. This component has

the ability to record up to 256 data about the temperature variations from the piezo-resistive transducers and electronic components.

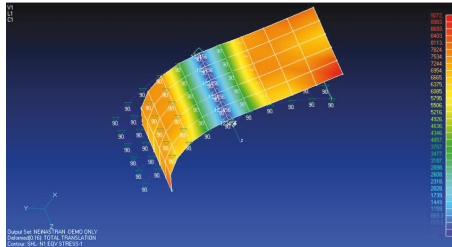


Fig. 27: Cantilever behavior under temperature variations between 18 °C – 45 °C.

The double cantilever was analyzed in FEA under temperature variation from 18° - 45° C. Figure 27 shows the temperature effects. It is possible to observe the symmetric behavior of the cantilever when two loads are applied; M_z and ΔT (18° - 45° C) with a reference of temperature of 21° C. This work makes use of the key factor of the opposite behavior of the two cantilevers. It uses the symmetric performance to substrate the strain in compression to the strain in tension, obtaining just the strain produced by the temperature's changes.

Figure 28 shows a proportional strain induced by $\Delta T = 0.5^\circ \text{C}$. The most important conclusion is that the strain in these areas is uniform and proportional.

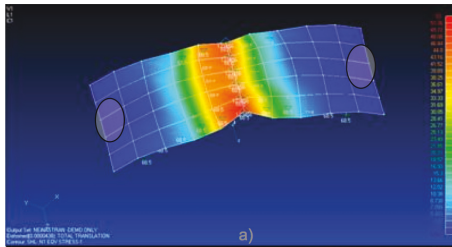


Fig. 28: FEA of double cantilever, increment 0.5 °C from reference temperature of 21 °C.

Figure 29 shows very small distortion at the strain level of the symmetry of displacement from both extremes of the cantilever. This could be the best position to attach the strain gauges.

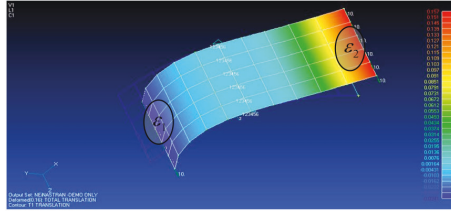


Fig. 29: ϵ_1 and ϵ_2 show symmetry in displacement under Moment .

If the sensing element simultaneously experiences both axial strain and a temperature change, the resulting strain is caused by a combination of both effects and can be separately identified (Tabib Azar, 1985)).

The mathematical process of temperature compensation is the following:

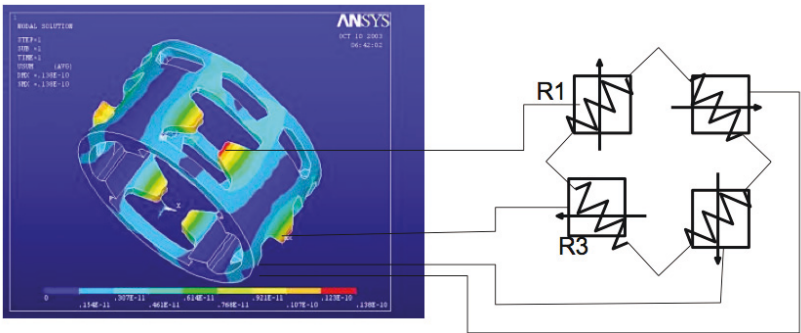


Fig. 30: Temperature compensation using Wheatstone bridge.

If ϵ_{esf} is the strain produced by mechanical load and

If ϵ_{temp} is the strain proportional to the temperature changes

and k is factor proportional to the position error of the temperature strain gauges

$$\epsilon_1 = \epsilon_{1_{esf}} + k_1 + \epsilon_{temp} \quad \text{Eq. 4.4}$$

$$\epsilon_2 = \epsilon_{2_{esf}} - k_2 + \epsilon_{temp} \quad \text{Eq. 4.5}$$

$$T_{comp} = \frac{\mathcal{E}1 - \mathcal{E}2}{2} \quad \text{Eq. 4.6}$$

$$T_{comp} = \frac{\mathcal{E}1_{esf} + k1 + \mathcal{E}_{temp} - \mathcal{E}2_{esf} + k2 + \mathcal{E}_{temp}}{2} \quad \text{Eq. 4.7}$$

$$T_{comp} = \frac{\mathcal{E}_{temp} + (k1 + k2)}{2} \quad \text{Eq. 4.8}$$

5. Design Evaluation

5.1 Sensitivity analysis of the strain gages position

To determine the best position of strain gauges over the sensor body, it was necessary to establish a relation between the load and the strain produced in x , y and z -directions. The results of this sensitivity analysis (plotted in polar coordinates in figure 31) show the correspondence between strain and angle, referenced from the Finite element results Strain data was measured at the nodes each 5° of angular degree. It is important to say that sensitivity analysis took just a few planar sections of the ring. It is possible to plot a three-dimensional sensitivity plot of the sensor body.

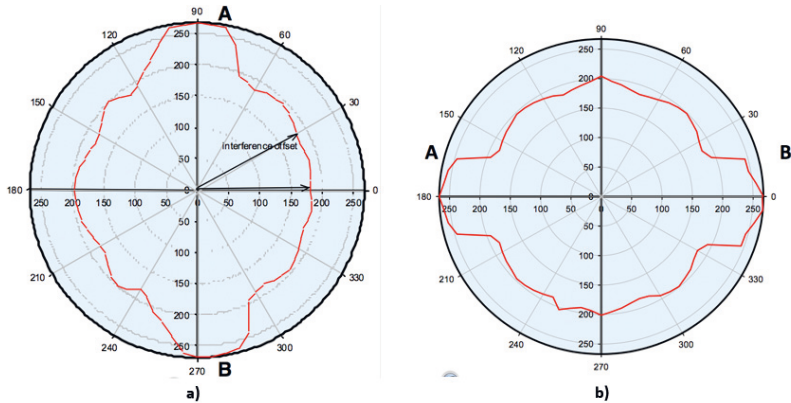


Fig. 31: The sensitivity plot from demonstrates that the best position to attach the strain gauges is at 0° (A) and 180° (B).

On the other hand, the sensitivity plot shows a high sensitivity at 90° (A), and 180° (B) of the sensor body. Also, this sensitivity graph shows important data about the level of transverse sensitivity. This interference could be eliminated with some multivariate analysis with the identification and discrimination of the relation between two or more variables, in this case load (M_x, M_y, F_x, F_y) and strain (as result) at defined angular position. In Figure 32 the sensitivity analysis shows high sensitivity at each cantilever beam. It is important to mention that the interference offset is less than the 20

% at each position of the surface. The principal components M_x , M_{xy} and M_{xz} and its respective interference values are shown in figure 32. The most important data is the maximum transverse sensitivity with a value of 10% of the maximum strain when the load M_x and M_y is applied.

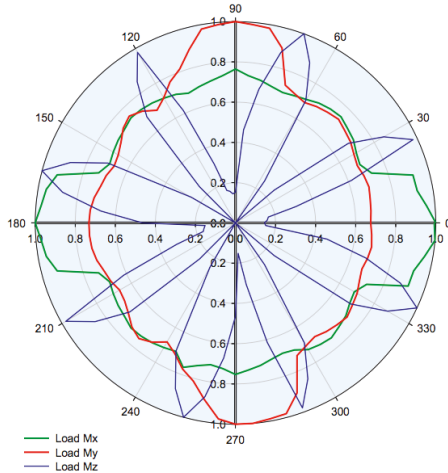


Fig. 32: Sensitivity analysis of the sensor body under moment in direction x, y, z . The most important data is the maximum transverse sensitivity with a value of 10% of the maximum strain when the load M_x and M_y is applied.

This transverse sensitivity is caused by the related component ($p \times f$) of the force applied. It could be reduced by symmetry of the load applied in grasping. Figure 33 shows the model of the force F_x and F_y applied direct to the sensor body. The maximum force has to be applied at the position of the central axis of the sensor body.

$$W = \left(\begin{array}{c} R^T f \\ R^T (-\rho \times f) + R^T \tau \end{array} \right) \quad Eq. 5.1$$

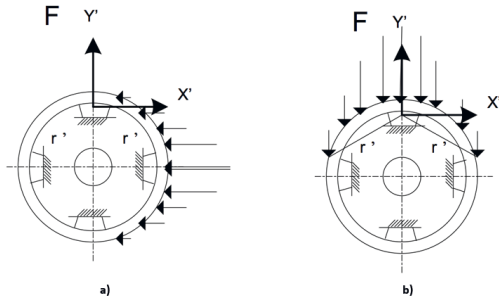


Fig. 33: Moment of interference caused by the of the applied force when are applied direct to the sensor body.

6. Mathematical definition of the sensor

The complete system is analyzed by the following mathematical model which is generated by the superposition of the whole effects involved in the sensor performance, such as mechanical performance of the structure, symmetry and materials homogeneities, mechanics of the adhesion (adhesive and cohesive), mechanics of the piezoelectricity and electrical relations of the Wheatstone bridge.

6.1 Mechanical component, structure, symmetry and material homogeneities

The structure and the mechanical coupling are influenced by its interaction with the fixed support inside of the sensor body.

$$\frac{M_{b(i)}}{EI_i} (z - z_0) \quad \text{Eq. 6.1}$$

with

$$i = x, y, z$$

where:

$M_{b(i)} = r \times F_i$ or *Moment produced by the force applied*

$I_i =$ *Moment of inertia*

$z - z_0$ *is the cantilever distance*

6.2 Mechanical symmetry and manufacturing

Symmetry is a crucial parameter for the sensor operation, hence the choice of the material, boundaries and manufacturing process are quite important to assure the same I .

6.3 Material homogeneities

It is possible to predict very fine and valid sensitivity models with mathematical and Finite Element analysis that express the variations and the effects of the transverse sensitivity at different regions of the sensor surface. It is important to have well defined properties and standardized material, assuring a regular and constant material properties.

6.4 Mechanics of adhesion

This is one of the most critical issues because it is responsible of the mechanical coupling and transmission of strain and deformation between the adhesive and the sensor body (aluminum surface). It is integrated by two functions, adhesive und cohesive mechanics.

$$kWD + \left(\frac{2E\gamma}{\pi a} \right) \qquad \text{Eq. 6.2}$$

6.4.1 Fracture

Bennett (1974) divided the concept of fracture in two, a) the separation of the strain gauges's adhesive from itself (cohesive fracture) and b) the separation of the adhesive from a dissimilar at the bond line between the strain gauge element and the aluminium (adhesive fracture).

Cohesive fracture

It is well known that an elastic stress singularity exists at a sharp geometric discontinuity such as wedge point, crack tip or edge of debond and depends upon the local boundary conditions loading and properties of the material (Bennett, 1974)

Griffith define the general equation of cohesive fracture as:

$$\sigma_{cf} = \left(\frac{2E\gamma}{\pi a} \right)^{1/2} \quad \text{Eq. 6.3}$$

With a finite critical stress that is a function of crack energy or accumulated energy.

This equation includes the adhesive fracture energy factor to predict the continuous mechanics of the fracture and the finite critical stress that is function of crack energy or accumulated energy.

Adhesive fracture

One of the most critical issues is the bonding process. The adhesive force must have a maximum value over the entire area. The mechanical locking or “anchoring” is the responsible for adhesion between the aluminum surface and the epoxic and between the epoxic and the piezo element. According to the manufacturer the adhesive must penetrate microscopic asperities on the aluminum and displace any trapped air.

The small scale contacts and very smooth surfaces result in adhesive forces playing a more significant role than in more conventional tribological applications. (Bennett, 1974).

The contact force is defined as:

$$F = kWD \quad \text{Eq. 6.4}$$

where:

W = work of adhesion or intermolecular interlocking work

D = Area of contact

k = Adhesive constant

Thus it is quite important to obtain the best performance of the adhesive (enhanced mechanical interlocking) and assure the quality of the bonding with the following actions:

- a. Clean surface, forming a highly chemically reactive surface for the best intermolecular interlocking increasing W .
- b. Mechanical abrasion chemical etching to increase the bounding surface area by roughing the surface increasing of the W

It is also important to have a deep understanding of the viscoelastic contact mechanics and the adhesion mechanics. This will reduce the share of the unknown in performance of the sensor.

6.5 Piezoresistive strain gauges

According to Robert Dunsch (2006), the physical behavior and the total strain of strain gauges is determined by a superposition of mechanical bending and deformation. It could be understood under the following equation:

$$\varepsilon_{tot}(z, x) = \varepsilon_0(z) + \frac{S_{11}^p}{EI} M_b(x)(z - z_0) \quad Eq. 6.5$$

where:

ε_0 is the strain that defines de bending

s_{11}^p is the compliance of the piezo material and

$$s_{11} = \frac{1}{2}(\pi_{11} + \pi_{21} + \pi_{44})\sigma_l + \frac{1}{3(\pi_{11} + 2\pi_{12} - \pi_{44})}\sigma_t \quad Eq. 6.6$$

$\pi_{11}, \pi_{21}, \pi_{44}, \pi_{12}$

are the principal components of teh piezoelectric tensor

M_b moment applied

6.5.1 Thermoelastic strain

Strain gauges are bonded for force sensing onto materials with dissimilar properties resulting in a thermoelastic strain. Most of the strain gauges are inherently unstable due to bond degradation, temperature sensitivity and hysteresis caused by thermoelastic strain. (Bennett, 1974).

The thermo elastic strain is defined as:

$$\text{div}[\chi(T) \text{grad} T] = \rho c \frac{\partial T}{\partial t} - H \quad \text{Eq. 6.7}$$

Where $\chi(T)$ denotes the thermal conductivity, ρ the mass density, c the specific heat. H accounts for the various heat sources and sinks in the system.

6.5.2 Wheatstone Bridge

The expanded relation that defines the Wheatstone bridge under the Taylor expression is the following.

$$\frac{\Delta R}{R} = C_1 \varepsilon + C_2 \varepsilon^2 \quad \text{Eq. 6.8}$$

7. System and construction

7.1 Manufacturing of the sensor body

The decision about the best option for the geometry of the sensor body was taken under Finite Element Analysis. This analysis considered “ideal conditions” about the homogeneities of material and geometry. Three elements – material, shape and symmetry are the critical factors for probing and for evaluating the performance of the sensor under real loads and conditions.

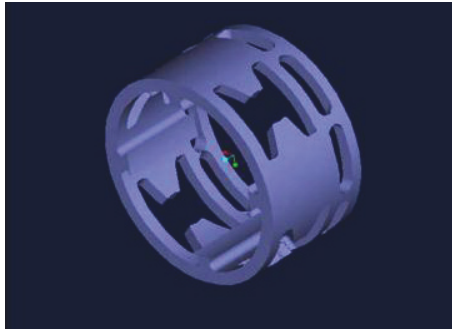


Fig. 34: Sensor body modeled under ProEngineer®

7.1.1 Geometrical form and symmetry

Manufacturing determines the accuracy of the mechanical performance of the sensor body. Procedures for high precision manufacturing applicable with comparably high quality were micro milling, electro-discharge machining, and laser cutting. Due to recommendations of Ilmenau experts, we decided to laser manufacture the sensor body - (low tolerances, good surface finishes, lowest costs). Figure 34 shows part of the manufacturing drawing of the first prototype.

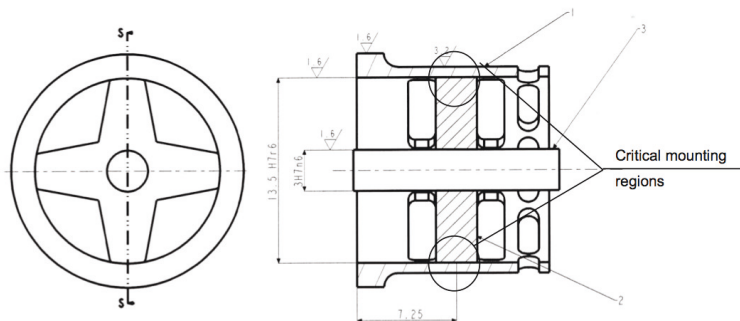


Fig. 35: Manufacturing version of the sensor body with indication of the critical region for the montage.

The most critical points are the assembly of the ring with the internal structure (supportive “cross”) and the montage of the internal structure with the central axis. If contact inaccuracies would appear between the internal support and ring the transmission of the mechanical stress could increase the hysteresis of the sensor, thus controlled press fit is necessary.

7.1.2 Material

Choice of the material is related to the first application in analyses on human and animal prehension. It is quite important to considerer material characteristics such as, low strength to ensure high mechanical sensitivity, humidity, chemical stability, temperature sensitivity, machinability and costs. This decision at present does not consider X-ray transparency. The information is resumed in the following matrix (figure 36 and table 2).

Aluminum 6061 T4 is a general purpose material. It has strength and elongation that are appropriate for the force measurement intended. On the other hand Aluminum 7075 O4 has excellent properties what concerns high fracture resistance. This property is quite appropriate to ensure the same mechanical performance for long lasting stress and temperature cycles. Moreover, this material exhibits a high chemical stability and it is recommended for harsh environments. Stainless steel has excellent chemo resistive properties but the formability is restricted compared to Aluminum 6061 T4 and with respect to Aluminum 7075 O4. Overall, Aluminum 7075 O4 is the material of choice.

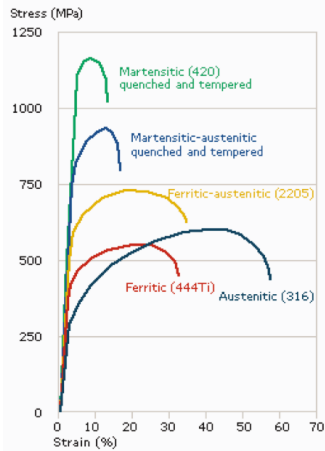


Fig. 36: Mechanical properties of stainless steels with different micro-structures (Kaiser Aluminum Corporation).

Tab.2: Matrix of the properties of materials

Material	Strenght (Mpa)	Elongation (%)	Chemical stability humidity	Fracture resistance (fatigue)	Formability
Non ferrous					
1. Aluminum 6061 T4	144.8 MPa	22%	Corrosion Resistance		Good
2. Aluminum 7075 O4	572.5 Mpa	11%	Harsh enviroment	High	Very good
Ferrous					
3. Stainless steel (ferritic 444Ti)	572.5 Mpa	11%	Harsh enviroment	High	Good

7.2 Transduction principle selection

The selection of the transduction must be in accordance with the objectives for the sensor. This means that use of this transducer must afford:

- a. The exploration of a high spatial integration over the sensor's body surface (very small size) and
- b. The exploration of high torque sensitivity (typical value: 50 mN).

According to table 3 four principles could produce positive results for these objectives: piezoelectricity, piezoresistance, capacitance, and inductance. Additionally we would aggregate optoelastic principles.

Tab.3: (Partial) matrix of transduction principle and energy form proposed by Grandke (1989): for mechanical energy five transduction principles may be chosen.

Transduction principle	Mechanical	Thermal	Electrical	Magnetic	Radiation
Energy			Piezoelectricity Piezoresistance		
Mechanical			Resistance Capacitance And Inductive effect		

Piezoelectricity has good sensitivity for strain and deformation, probably a piezoelectric transducer from Polyvinylidene Fluoride (PVDF) could be useful especially for detection of dynamic forces (Yantao, 2008).

Piezoresistance exhibits a high gauge factor, fifty times higher and thus more sensitive than copper wire resistive strain gauges. Moreover elements with piezoresistance are exploited in a variety of research and commercial applications. It is possible to find very small elements in commercial form at the market. The most critical limitation is the temperature dependence (internal and external) that directly affects the gauge factor.

Capacitance and inductance effects are quite interesting effects but in this application could complicate the simplicity of the sensor design.

As the result of a systematic evaluation, piezoresistive strain gauges are the most adequate and the most reliable option for the task to be carried here.

7.2.1 Piezoresistance effect

Mechanical stress induces a change in the energy band structure, this effect is reversible within the elastic region (Keyes 149-221). The mechanical disturbances (stress in a silicon piece) provoke changes on carriers in silicon, As mechanical stress induces a reversible change in the energy band it produces a repopulation of the carriers in silicon into its elastic range (Kanazawa and Gordon 2004).

In non degenerate n-type silicon, the stress induces a repopulation of electrons in the conduction band. This gives variations in the isotropic electron mobility as a result of the different electron effective masses. In p-type Si, the dependence of resistivity on stress provokes a repopulation between heavy and light holes in the valence band.

According to the present knowledge about the stress components, the fractional change of resistivity in a piezoresistive layer can be evaluated (Kanazawa and Gordon 2004).

Exploiting the symmetry conditions and the principal coordinate system of cubic silicon, there are only three linearity independent components. This mathematical model describes the interactions of electrical and mechanical phenomena. The relative change of resistance can be expressed as:

$$\frac{\Delta R}{R} = \frac{1}{2}(\pi_{11} + \pi_{21} + \pi_{44})\sigma_l + \frac{1}{3(\pi_{11} + 2\pi_{12} - \pi_{44})}\sigma_t \quad \text{Eq. 7.1}$$

Here σ_l denotes the average of the normal stresses in longitudinal (parallel) and σ_t the transverse direction (perpendicular) of the current flow. The coefficients $\pi_{11} + \pi_{21} + \pi_{44}$ are the principal coefficients. The equation does not account for the effects associated with shear stress and cross terms. Depending on the resistor geometry and orientation these effects can be neglected.

The equation does not consider the nonlinearities provoked by the higher order of the piezoresistance coefficients and stress terms. Besides detecting induced stresses by piezoresistive effect, some capacitive effects are associated with the deflection of the geometry.

7.2.2 Strain Gauges

On the basis of its operating principle, strain gauges can be defined as a measuring device on sensor, which applied on the surface of a test structure, produces an electrical resistance variation that is proportional to the strain to which the structure is subjected (Baumann, 2006).

On the other side the temperature gradient influences the transport equation (Grandke, 1989) in Si. This equation includes a component of electric current density with the temperature gradient as driving impulse.

Electrical and thermal interactions in the device can be accounted by an additional heat flow equation

$$\operatorname{div}[\chi(T) \operatorname{grad} T] = \rho c \frac{\partial T}{\partial t} - H \quad \text{Eq. 7.2 = 6.7}$$

Where $\chi(T)$ denotes the thermal conductivity, ρ the mass density, c the specific heat. H accounts for the various heat sources and sinks in the system.

An elaborate account of the temperature dependence of the various terms in the transport relations can be found (Selberherr, 1984). Experimental data limits the maximum operational temperature in the range of $-100\text{ }^{\circ}\text{C}$ to $100\text{ }^{\circ}\text{C}$ to achieve accuracy and a linear performance of the piezoresistance coefficients.

On the other hand a strain gauge exhibits a current carrying capacity. The maximal permissible current in bonded piezoresistive elements is controlled by the mechanism of heat dissipation. Therefore it is important to have current limitations with a maximum operation power of 0.1 W . (Window, 1992)

For a strain gauge with a resistance of $350\ \Omega$ the maximum current can be calculated as:

$$W = i^2 R \quad \text{Eq. 7.3}$$

$$i = \sqrt{\frac{W}{R}} \quad \text{Eq. 7.4}$$

$$i = \sqrt{\frac{0.1}{350}} = 0.0169\text{ A} \approx 17\text{ mA} \quad \text{Eq. 7.5}$$

7.2.3 Gauge selection

Based on the selection of the strain gauges parameters, a search was made to find commercially available piezoresistive gauges under two criteria, a piezoresistance with a high gauge factor and dimensions between 1 and 2 millimeters. The strain gauges ESB-020-500 from ENTRAN, meet completely these two criteria, a gauge factor equal to 150 and a dimension about 1 mm. The general specifications are shown in figure 37.

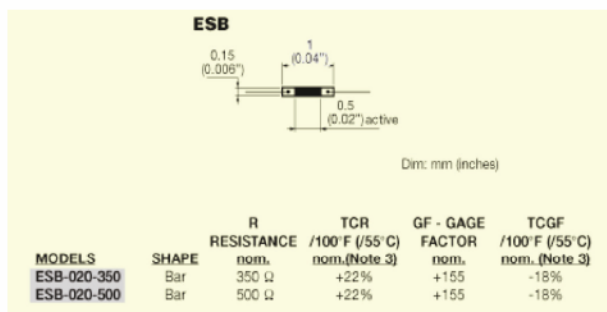


Fig. 37: Strain gauges dimensions and characteristics from the ESB models from Entran.

The ESB-020 is a bar P-Type, (111) with a nominal resistance of 500 Ω, and a nominal gage factor of 155. The manufacturer recommends of 0 – 100 μstrain for the best performance with a maximum interval of 0 – 300 μstrain. A presumable complication with ESB-020 could be the bounding because of its size and restricted manipulation possibilities. Lamentably there is not a self-bounding commercial product with these dimensions at the market.

7.2.4 Bonding process

Since bonding is a superficial phenomenon it is primordial to understand both 1) the interactions between the adhesive (epoxy) and the surface of the aluminum, and 2) the interaction from the adhesive and the piezoresistive element.

7.2.5 Adhesive theory

In the study of adhesion, the equivalent observation is the spontaneous jumping of smooth surfaces into contact (Perrin, 1923). Two ultra-smooth pieces of mica, gold, polymer or solid gelatin solution cannot be held apart when their separation becomes small enough, typically 1 nm to 10 nm. Such attraction is impossible to explain by electrostatic, magnetic, or gravitational forces, which act from the center of bodies and obey the inverse square law (Bennett, 1974). These forces that can be detected at much greater distance are more similar to surface tension, a short range surface force that can be changed by a single layer of molecules laid at an interface.

The maximum force is the adhesion force. This adhesion can be explained by the molecular adhesion evidenced mechanical mechanism linking adhesion force and molecules (Kendall, 1994).

Also Kendall (1994) defines the work of adhesion as the energy per unit of area multiplied by the area of contact from the surface attraction. He explains that this work can be tough as 99% of van der Waals forces. The other 1% is responsible for resp. due to the ionic and covalent forces.

Israelachvili (1985) calculates the mechanical force F and work of adhesion W needed to separate two identical spherical particles of diameter D from molecular contact. This equation is:

$$F = kW D \qquad \text{Eq. 7.6}$$

where k is a constant near to unit.

This equation interconnects the mechanical and the chemical attraction with spherical surface representation of the adhesive ending molecule chains that interact with the asperity of the metal, this interaction is named by “the mechanics of adhesion” (Bennett, 1974).

Besides of attraction force, (Bennett, 1974) defines the concept work of adhesion as the work required to separate the interference (adhesive) area whatever its physical origin. This could be intermolecular forces, electrostatic forces or capillary action. For elastic solids the behavior is a function of two non-dimensional parameters. (Bennett, 1974) defines two ratios:

- a. A measure of the relation between of the adhesive force to the applied load.
- b. The relation between elastic deformation to the range of surface forces.

The effect of inelastic deformation (plastic and viscoelastic) is not considered in this work.

7.2.6 Adhesive selection

The manufacturer of ESB-020 recommends an epoxy adhesive or phenolic resin (M-Bond 610). This adhesive shows high stability after the cure process to a maximum temperature of 180 °C. There is neither much information about the mechanical performance of the M-Bond 610, nor enough information about creep. These are the properties specified by the manufacturer:

Elongation capabilities : 3% from the room temperature

Epoxy phenolic resin: Operation temperature (-269 °C to 370 °C)

Surface preparation for bounding strain gauges

The main purpose of the preparation is cleaning the surface to ensure a highly chemically reactive surface and ensure a mechanical abrasion on the surface to provoke the maximum interaction between the aluminum and the surface (sphere molecule model).

Cleaning will decontaminate the surface from superficial chemicals. This action is performed with solvents recommended by the manufacturer. On the other side, mechanical abrasion makes a rougher surface ideal for a maximum force of adhesion. The manufacturer recommends a roughness between 2 µm and 4 µm.

The procedure for the preparation includes:

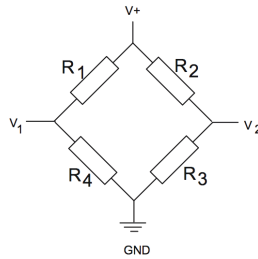
1. Application of solvent,
2. Cleaning the surface with a second chemical and
3. Mechanical abrasion to obtain the adequate roughness.

7.3 Electronics

The following elements are commonly found in data acquisition systems (DAS) (Taylor, 1997): signal conditioning that includes all the devices for converting the signal from the sensor to the correct level for the A/D. DAS includes amplifiers, filters, and A/D converters, anti-aliasing filters for removing high-frequency. The A/D is the central part of the system which requires a stable reference voltage and stable clock time pulses.

7.3.1 Wheatstone bridge

Wheatstone bridge is used for precision measurements of small resistance changes. The bridge arms define an equilibrium relation of the voltage between the two resistance arms. Small changes in resistance produce differential changes of the voltage. The mathematical relation of the bridge is expressed in equation figure 38.



$$I_1 R_1 = I_2 R_2$$

Eq. -set 7.A

$$I_1 = I_3 = \frac{E}{R_1 + R_3}$$

and

$$I_2 = I_4 = \frac{E}{R_2 + R_4}$$

$$\frac{R_2}{R_2 + R_4} = \frac{R_1}{R_1 + R_3}$$

$$R_4 R_1 = R_2 R_3$$

Fig. 38: Wheatstone bridge and its mathematical definition.

7.3.2 Nonlinearities of the Wheatstone bridge

Although the Wheatstone bridge gives maximum sensitivity it is possible to find some inherent nonlinearity in the performance produced by a second order constant from equation 25

$$\frac{\Delta R}{R} = C_1\varepsilon + C_2\varepsilon^2 \quad \text{Eq. 7.7}$$

where C_1 and C_2 are constants and ε is the strain

This equation influences the linearity and the sensitivity of the measurements. Kreuzer (2004) explains that a current fed circuit could improve the stability and the sensitivity of the Wheatstone bridge.

7.3.3 Temperature compensation

One important question about the temperature compensation is how to distinguish and separate the effects of temperature variation produced by an internal source (self-functioning) from the effects provoked by an external source. The answer to this question clarifies two methods of compensation, the first a self-compensation and the second a circuit (general) compensation. The self-compensation involves the *zero shift or apparent strain* and Gauge factor variation.

- a. Zero shift is an observed offset of zero stress. This could be reduced with well matched push-pull gauges (Neubert 2002) and with the integration of a temperature sensor to measure and register every temperature change.
- b. Gauge factor variation. This is the variation of the gauge factor produced by elevated temperatures. This effect produces an increase of gauge resistance. Its loss of sensitivity could be reduced if the gauge current is constant. This is the reason why each sensor needs a signal conditioner component, designed for having a very stable current source especially with the temperature variations Wheatstone

bridge. This issue could improve considerably the accuracy of the sensor node.

After a search over commercial Wheatstone bridge conditioners MAX1457 (producer

MAXIM) was chosen with two properties, a very stable current source for powering of the bridge and an integrated temperature sensor to measure the temperature of the system. This component incorporates a memory EEPROM to record 256 temperature variation of temperature.

7.3.4 Complete configuration of the system

The complete configuration is composed by the configuration of the sensor node and by the components that sensor nodes share.

Configuration in figure 39 allows the attaching the Wheatstone bridge, signal conditioning, filtering and microcontroller into the sensor body. This sensor unit will be ready to connect other sensor units and transfers data to the slave.

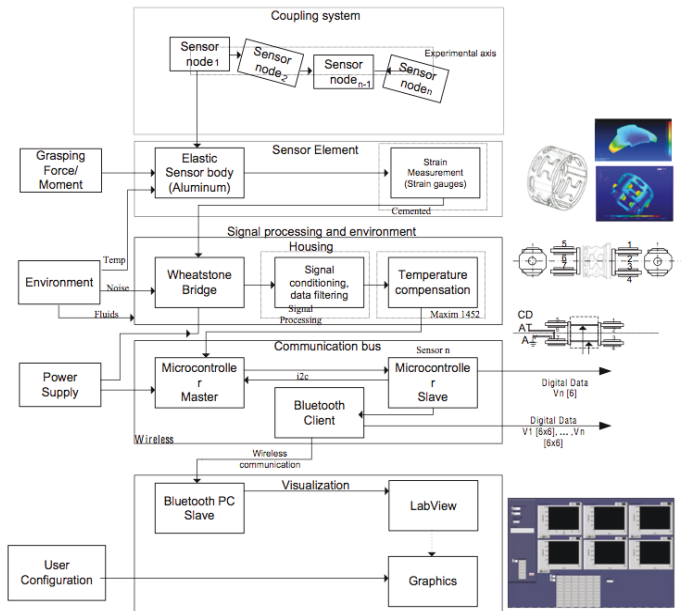


Fig. 39: Sensor configuration.

Figure 40 shows the main components such as 1) six full bridges with 6 signal conditioners. The small PCB 12 mm are positioned by pairs and share power supply 5V and GND. 2) Connectivity bus to transfer data between both sides of the electronic configuration, 3) Microcontroller unit programmed with master mode to have control of

the communication and transmission of data 4) I2C Bus. This protocol reduces the space for cabling using 2-line channel for data (CData) and channel for clock (CLK) communication bus.

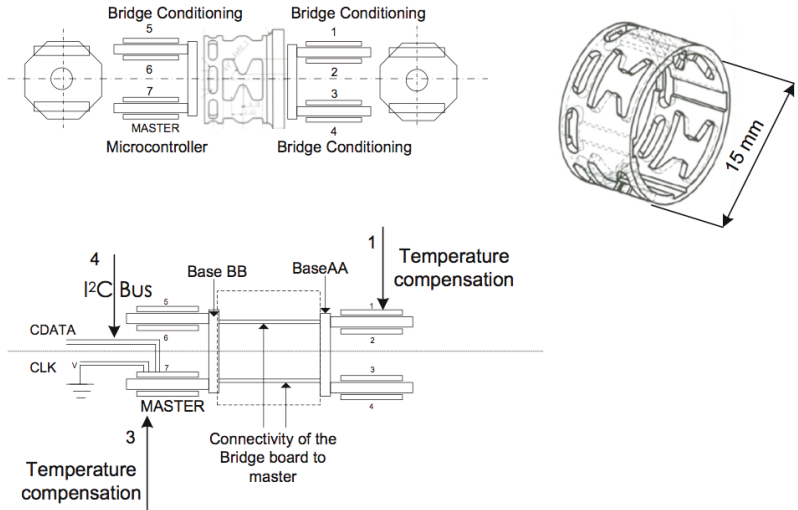


Fig. 40: Inside of the sensor node configuration. a) Electronic board configuration and b) board connectivity.

The complete structure is represented in figure 41. The sensor body is the effector for the external force and moment. Its energy is represented in strain measurement by the 24 bonded gauges on the surface. Six Wheatstone bridges detect small changes of resistance of the strain gauges. Each full bridge is doted by a signal conditioner that ensures a stable current source and temperature compensation. The six electrical signals $[\epsilon_1, \epsilon_2, \epsilon_3, \epsilon_4, \epsilon_5, \epsilon_6]$ are pre-amplified inside the sensor and digitized by the microcontroller in master mode. The corresponding six signals are sent and recorded in one "package" (address of the sensor node plus the six signals) to the slave microcontroller via the *P.C*. Finally the slave sends the signals to the computer via a wireless Bluetooth connection.

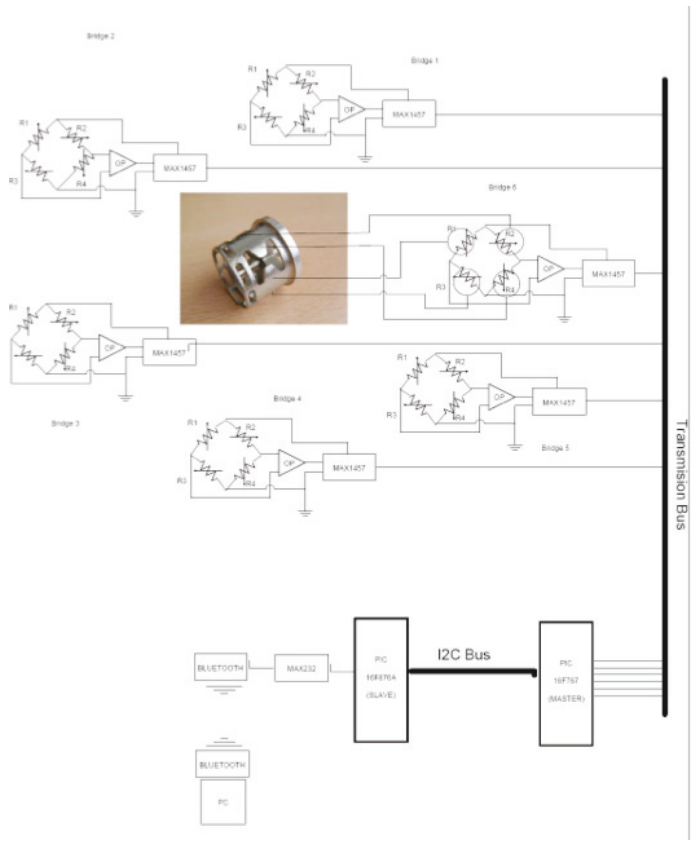


Fig. 41: The complete configuration of the Wheatstone bridges.

7.4 Communication in I^2C

The communication system is a serial bus, *a bus comprises a number of wires carrying related signals and each connected to several devices* (Taylor, 1997), that transfers the address of the sensor node plus the order of read or record plus the signals of $[\epsilon_1, \epsilon_2, \epsilon_3, \epsilon_4, \epsilon_5, \epsilon_6]$. Information is associated, classified and processed by the slave. It knows the address and the channel of each data. Channel 1 is identified as the

signal from bridge F_x . Channel 2 is identified as the signal collected from bridge F_y and so forth, channels 3,4,5,6 are identified as the signals collected for F_z, M_x, M_y, M_z . The slave is able to detect and receive information of 7-bit address microcontroller with a limit of 112 sensors. Figure 42 shows the sequence on the I^2C

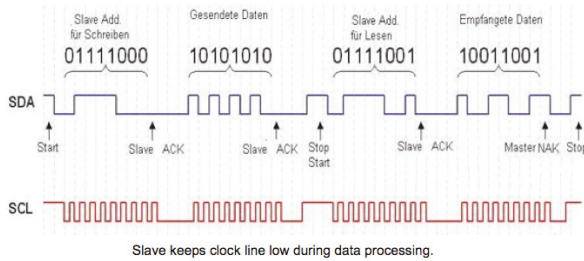


Fig. 42: I^2C Communication system of the multi node sensor system.

The master converts signals from analog to digital in a 10 bit word. The resolution of the system is about:

$$Resolution = \frac{5V}{1024} = 5mV \quad \text{Eq. 7.8}$$

7.5 Cabling

Cabling is a critical aspect to consider because the cables reduce space inside the sensor body by a factor of 8. An increased number of soldering nodes could cause additional noise at the output signal of the sensor. It is common to see thermoelectric voltages as the most common source of error in low level voltage measurements such as Seebeck effect or Thomson effect. Seebeck effect is the flow of current produced when the junctions of a circuit made of two different metals are at different temperature (Granke Thomas, 1989). The Thomson effect describes the production of an electromotive force inside two points at different temperatures (Granke Thomas, 1989). Each metal-to-metal junction generates an electromagnetic force proportional to its temperature, therefore it is important to take some precautions to

minimize thermocouple voltages because the strain gauges have a gold connection and they have to be connected with copper by soldering.

7.6 Housing

Every measurement system responds to its total environment (Wilson, 2005). Therefore it is very important to select the right geometry and material for protection of the internal functionality of the sensor. Additionally must be considered the influence of the changing conditions of the ambient, for example the change of acceleration into sensitivity and zero shift. It is important to consider also, some internal compensation for the acceleration when the application involves important dynamic effects, vibration or shock.

The housing must be resistant to moisture, corrosion and humidity (animal fluids). The design of a hermetically sealed housing could protect and isolate the electronic boards but could otherwise increase the internal temperature of the components.

8. Results of the prototype and integration

Each single component of the sensor was thought not only for its particular function but also for its global functionality. The integration process implies the most of time and work in order to produce satisfactory results. Integration is more than just manufacturing elements and put them together, we pursued to produce an interconnected system, creating a global functionality about the manufacturing and mechanical montage, the transducer and bonding process, the electronics and microcontroller *PC* and the Bluetooth and the computer visualization.

8.1 Manufacturing and Montage of single elements

Integration of the sensor underlies the following order, 1) Manufacturing of the sensor body, 2) Surface preparation 3) Strain gages montage, 4) Cabling, 5) Montage of the electronic boards, 6) Assembly to the probe form, 7) Connection with Bluetooth, 8) Computer visualization, and 9) Calibration.

8.2 Manufacturing of the structure of the sensor body

Some parameters impact positive and also negative the performance of the sensor. Some of them, such as precision and symmetry, have enormous relation to the mechanical performance of critical regions such as the internal montage (figure 43). Moreover material homogeneities influence specially hysteresis, cracking of the surface and symmetry of the mechanical response, including stresses and deformations. These are enough reasons why is important to put special attention at the manufacturing process, especially in the sensor body.

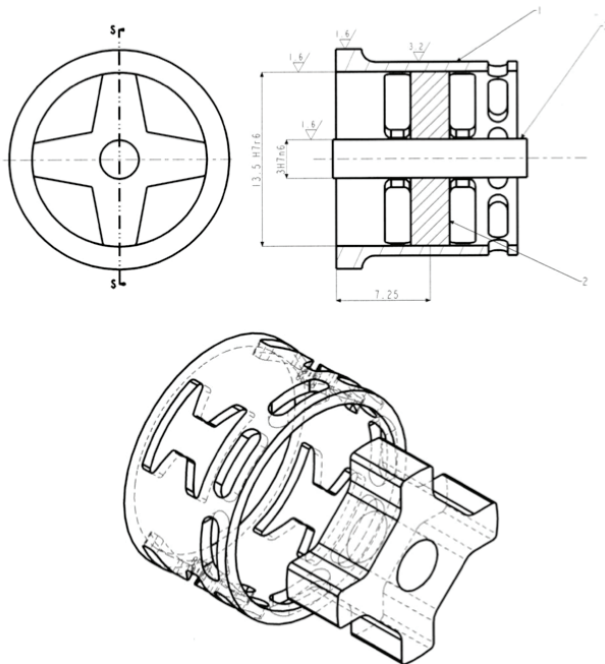


Fig. 43: Inside of the sensor design. Drawings of the sensor body and its montage.

The body of the sensor prototypically was produced at Ruhr-Universität Bochum with a high precision CNC machine under the described specifications. The prototype is shown in figure 44.

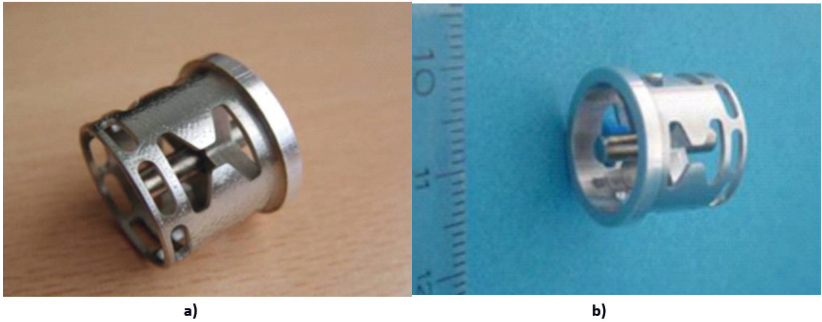


Fig. 44: Prototype of the sensor body.

8.3 Surface preparation

It is important to obtain the best performance of epoxy to enhance mechanical interlocking. With two tasks we can assure the quality of bonding:

- a. Cleaning surface, forming a highly chemically reactive surface for the best intermolecular interlocking- increasing the work of adhesion (W), removing influence of smoothing contaminants such as grease or dust.
- b. Mechanical abrading to increase the bounding surface area by roughing the surface increasing the work of adhesion (W). We tried to produce a high performance sensor as result of detailed task summary, putting more and more attention into the fine aspects of the design and in the phenomena involved. In this case, the adhesion mechanics of micro-scale contacts and surfaces.

To avoid disturbances and conductivity in each electrical connection an isolation layer (electric pre-shield) of about 0.1mm was put on surfaces. We deposited a sprayed adhesive layer using a rotating system shown in figure 45. This layer was cemented for two hours at 145° C.

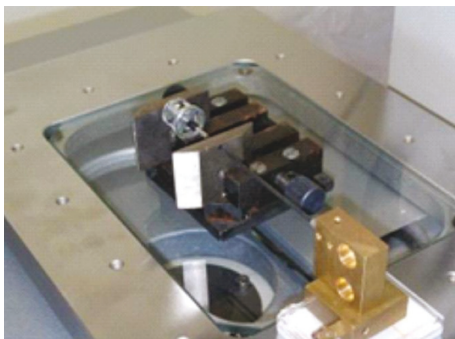


Fig. 45: Rotating and positioning system.

8.4 Strain gauges montage

The montage of the strain gauges was critical and complex task. It was necessary to use the support of a microscope for the positioning of each strain gauge. Various problems appeared at this stage. One of the most complicated was the stabilization of the position of the strain gauge during cementation process. The temperature of the oven provoked changes in equilibrium between the adhesive and the gold cabling of the strain gauges. As M610 adhesive is a fluid the cabling produced a moment stronger than the effect of the attractive forces of the adhesive, changing the position of the strain gauges. This change produced a position error of about 3° - 4° of the desired position shown in figure 46.

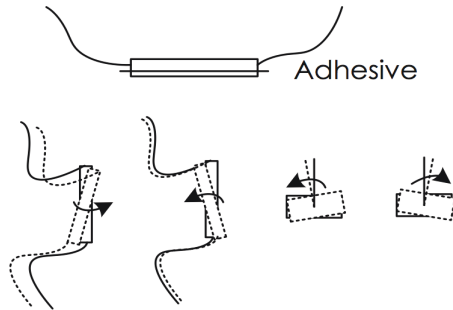


Fig. 46: Error in position of the strain gauges caused by cementation process.

The unpacking and the uncontrolled longitude of the gold cable produced problems in the montage. Figure 47 illustrates dosification's problem of the adhesive and of the control of positioning of the gauge. The figure shows the angular orientation error with respect to the exact position planned on the surface.

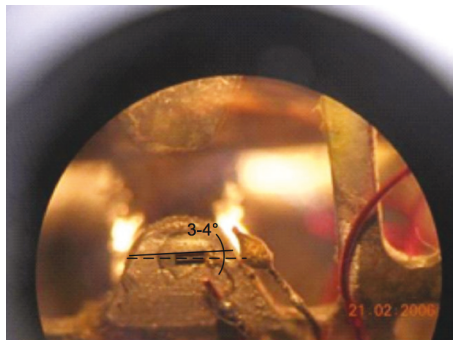


Fig. 47: Position error during attachment of the strain gauge at the planned position.

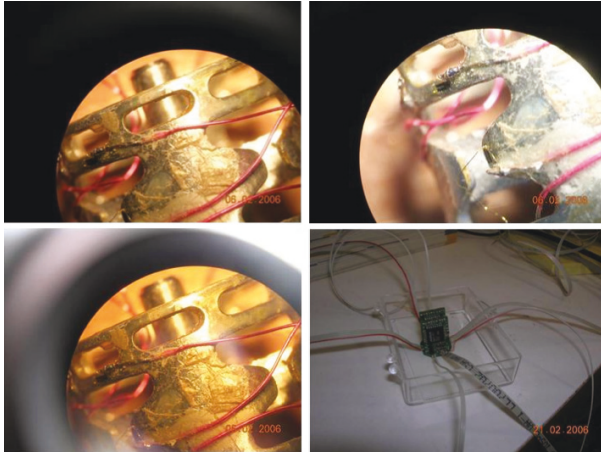


Fig. 48: Integration of the full Wheatstone bridge.

After each of the 24 strain gauges montage, it was necessary to solder each cable in order to integrate the six full Wheatstone bridge. Figure 48 and 49 shows the final montage and soldering of the 24 gauges.

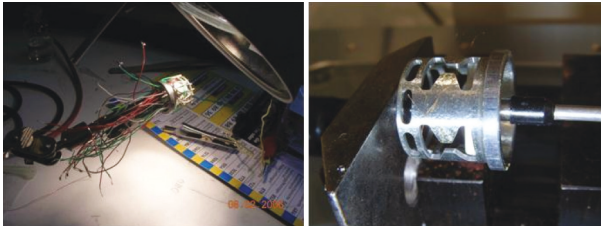


Fig. 49: Each sensor carries 24 strain gauges. The figure compares the situation after mounting to the raw sensor body.

8.5 Montage of the electronic boards

Montage and soldering of the electronic boards increase the complexity of the manufacturing because of the limited space inside the sensor body. It was not possible to put all the electronic inside in the first prototype. The experience taught us that the order of the montage of components has to begin with the coupling of electronic boards, before the beginning of soldering processes. Figure 50 and 51 illustrate the assembly of electronic boards.

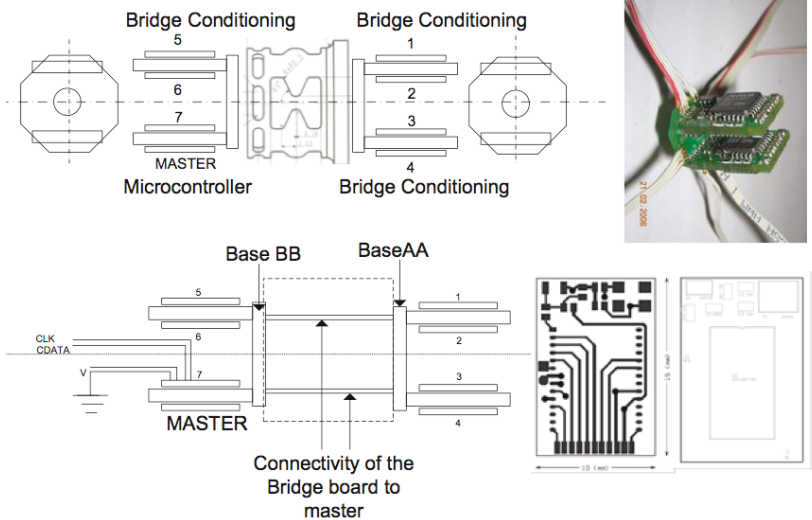


Fig. 50: Final assembly of electronic boards. Inside of the boards the microcontroller and the signal conditioners are placed.

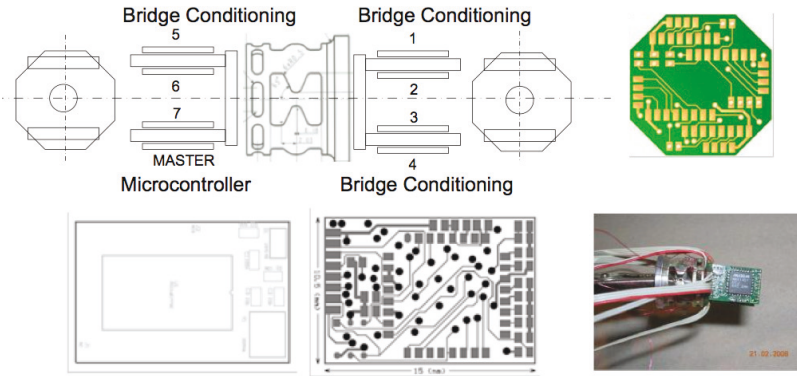


Fig. 51: Final assembly of the electronic boards with dimensions about 10.5 mm x 15 mm.

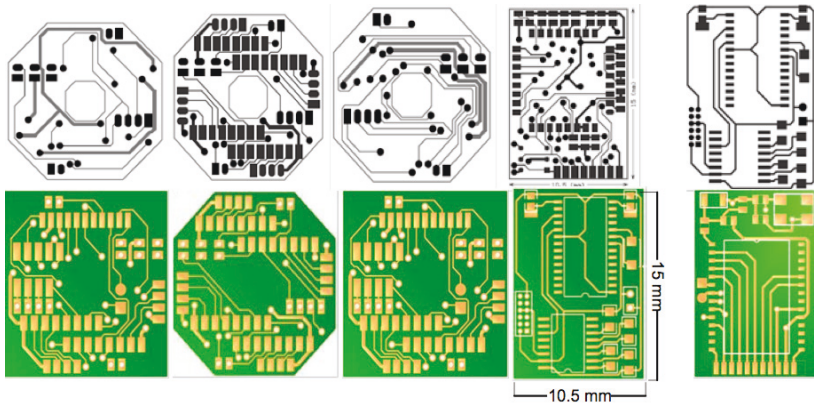


Fig. 52: Electronic boards designed for SMD402 elements.

8.6 Assembly of the sensor

Each single part of the sensor was assembled in one simple piece, like shown in figure 53. This configuration simplifies the operation and calibration of the sensor.

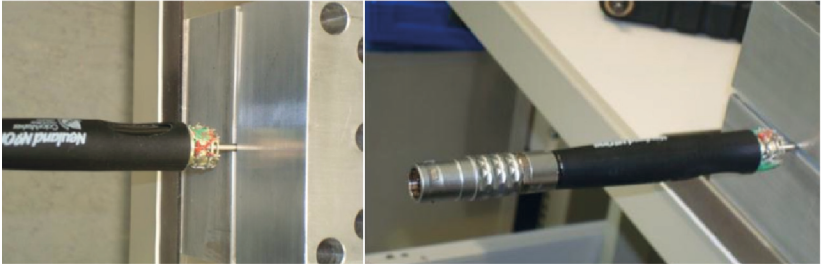


Fig. 53: Final assembly of the sensor body with 24 strain gauges.

8.7 Visualization in Labview

Visualization in Labview of each of the signals of forces and moments in direction x , y , z was the last stage of the integration process. The visualization window, shown in figure 55 and 56, puts together the information of each signal received by the micro-controller and by the Bluetooth channel.



Fig. 54: Visualization in Labview.

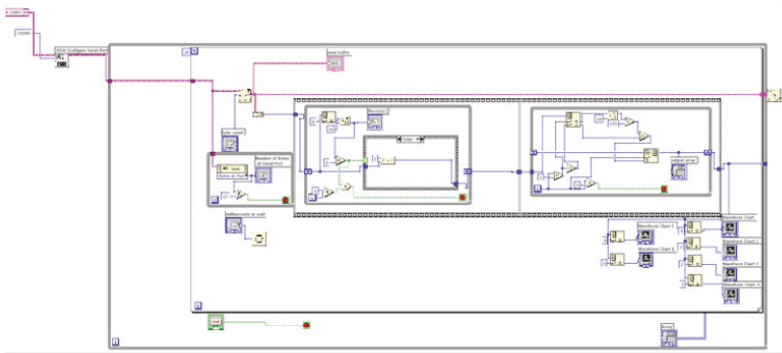
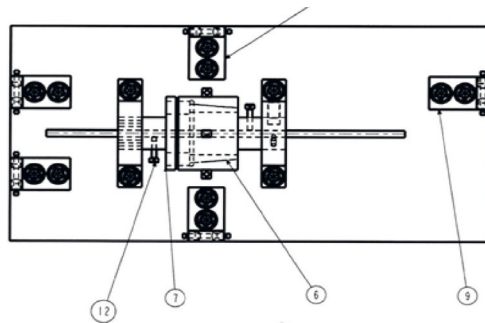


Fig. 55: Labview signal processing.

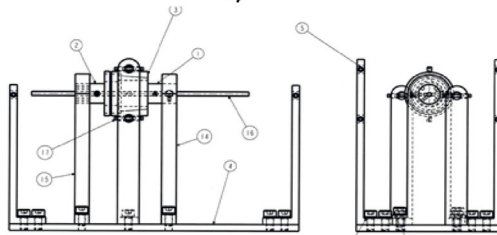
8.8 Calibration system

Good calibration design is extremely important in order to obtain the enough amount of useful information from a sensor (Naes & Risvik, 1996). They define the success of the sensor, satisfying completely the objectives of the sensor. It is important to have a careful execution of the experiment to detect and to eliminate the systematic errors and the non-systematic errors based on a careful analysis of data.

Figure 56 and 57 shows the framework of the calibration system. It includes a small base to attach and fix the sensor. The principal idea is to apply standardized weights in different directions and configurations to induce forces and moments to the sensor. This system could be a useful solution to prove the general characteristics of the sensor. It is important to consider a complete sensor's characterization under a professional standard's office to obtain a calibration datasheet from a more than prototypic sensor.



a)



b)

Fig. 56: Scalable design of the calibration system.

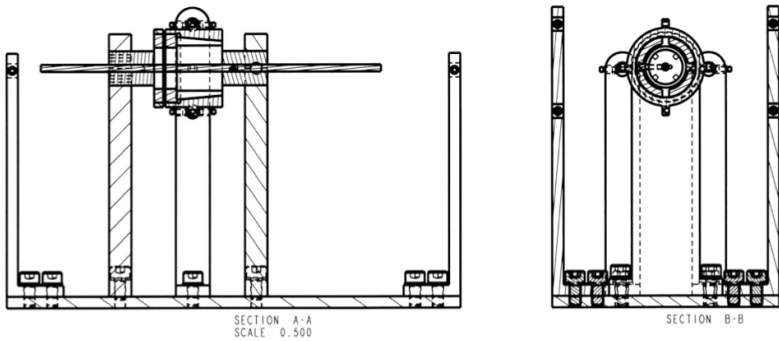


Fig. 57: Section through the calibration system.

8.9 Calibration procedure

The calibration procedure was performed following the diagram shown in figure . The most important objective of this procedure pursued to define traceability with a reference patron or standardized weights. The diagram shows the application of 8 different weights at three different times (t_1, t_2, t_3) under two different temperatures (T_1, T_2) and under two basic pre-states (C_{sf}, C_{sm}). The data obtained was analysed to obtain the principal characteristics of the sensor defined in the next chapter.

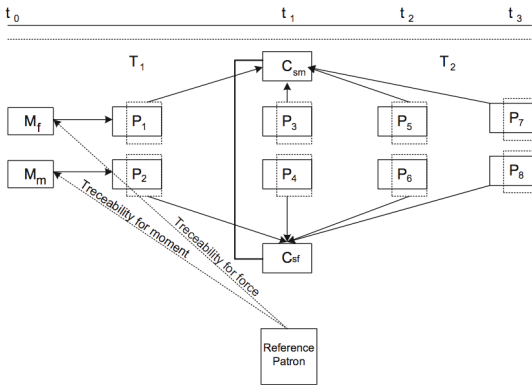


Fig. 58: Calibration procedure assembly and diagram.



a)



b)



c)

Fig. 59: Tools used for the calibration (a) Standardized weights used for the calibration process. (b) Standardized weights used for the calibration process. (c) Devices for reference of the moment and temperature.

9. Sensor data sheet

The sensor data sheet expresses the characteristics and performance of the force-moment sensor which was probed under various conditions and loads. With reference to Chapter 3, the following characteristics were determined.

1. *Accuracy.* The sensor shows an error = 19.3 mV at FSO. This provokes an inaccuracy equal to $\pm 4\%$ of the FSO. It is possible to improve this value defining the quantity, quality and performance of the imprecision sources. In this case the most important source was at the montage of strain gauges because of three main reasons, a) for the absence of the assurance procedure for bonding procedure to determine the exact position and orientation of each strain gauge, b) for the mechanical montage of the intern support of the ring (the cross) with the geometrical ring and c) for the differences of the adhesive layer at each position of the surface. With some mechanical design modifications it is possible to avoid or reduce these positioning errors at the montage of the strain gauges. The sensor body could have printed the exact position of the gauges. This mechanical coupling inaccuracy could be reduced under a synthesis analysis to reduce the components from two parts into a sensor body made of one piece.
2. *Precision.* The sensor demonstrates a precision equal to 2% FSO. The two temperature compensation mechanisms improve the accuracy of every measurement. The system does not consider vibrational and impact alterations, it considers just temperature as the main disturbance effect. The electronic components show a stable performance.
3. *Resolution.* The smallest increment in the value of the measurement was 10 g/mV.
4. *Sensitivity.* This aspect refers to the slope of the best fit line. This term is equal to about 0.4 mV/g. The system demonstrates a small sensitivity that could be produced by a mechanical coupling of the sensor with the prototypic pen-application.
5. *Selectivity.* $S = 0.08$ (8%), this characteristic quantifies the important relation between the temperature and the output of the sensor.
6. *Threshold.* This value could not be determined because the weights of the standard do not provide sufficient resolution.
7. *Nonlinearity.* Figure 9 2 shows the nonlinearity of the sensor: at the worst case it

is about 8% FSO. This value fits to the design goal which is a maximal non-linearity of 10 %.

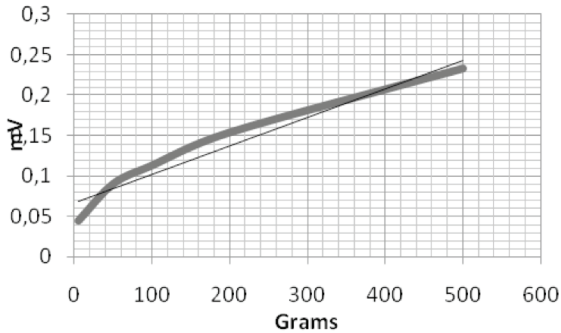


Fig. 60: Linearity for standards weights of 10, 20, 50, 100, 200, and 500 grs. applied in direction

8. *Threshold.* The value obtained was 5 mV.

9. *Conformity.* The best fit line was

$$y = 0.003x + 0.0683 \quad \text{Eq. 9.1}$$

$$R^2 = 0.9545$$

95.45 % of the values are represented by this linear relation.

10. *Repeatability.* It is about 98% of the FSO.

11. *Span Operating full range.* 0 N 4.905 N (equivalent to a weight of 0 g - 500 g) and 0 mN - 150mN.

12. *Output impedance.* It is about 208 Ω

13. *Grounding.* The system does not have any especial consideration

14. *Isolation.* Filtering from 50 Hz - 60 Hz.

15. *Instability.* The sensor shows a strong relation with the temperature, especially with gauge factor variations of the piezoresistive material.

16. *Power Consumption.* 18 mA.

10. Discussion of critical issues

10.1 Understanding the energy flow

The mathematical model of sensor defines with accuracy the relation among variables that describe the performance of each process mechanically, electrically and electronically in the sensor. This model makes possible a fragmentation of the total effect into separated effectors or fragments. The understanding of the performance of the micro effects, for example the mechanics of adhesion, could clarify the global performance and the mechanical transmission of the stress between the two frontiers, the surface of the aluminum with the adhesive and the frontiers of the adhesive with the strain gauges. In this sensor those seemingly trivial aspects become transcendent in obtaining the best possible performance.

One of the most useful applications of a model of a physical system is in simulating the behavior of that system, to avoid the need to construct the system iteratively (Grandke, 2004). Perhaps even more useful is the ability to determine the effects of variations of the model parameters to the system performance. In an actual sensor system, it is not possible to have access to all of the parameters, and vary all of them to fully characterize their effects.

Having an accurate model of the system and knowing the measurement configuration, it is possible to calculate these characteristics. This is called a sensitivity analysis of a system. If some of the parameters change, then we can calculate the effects on the performance of the sensor. (cf. Potter, 2003).

10.2 Simplicity

Simplicity appeared as design criteria easy to reach, but it was not. The simplification of the sensor's tasks such as components design, geometry, transducer's montage or communication system, needs a deep process of synthesis to reduce and integrate parts of different nature into a one harmonized function.

10.3 Knowing the variable to measure and the variables that influence the sensor performance

Knowledge about the undesirable variables defines the grade of control of uncertainties and the control error as part of the output. The understanding of the uncertainties became a pillar in the design criteria of reliability and accuracy for a force sensor. The concept of “just a force sensor” includes the concept of a force sensor able to measure others variables as temperature with accuracy as well.

„Sehr wichtig ist die Frage der Linearität von Umformung und Umsetzung. Wegen häufig nicht linearen Messglieder (besonders der Fühler) sind die Messsignale in ungewollter Weiser verfälscht. In diesen Fällen sind für die Korrektur entsprechende Messsignalverarbeitungsmassnahmen notwendig, die zu dem gewünschten Resultat, dem linearen Zusammenhang zwischen physikalischer Größe und Anzeige, führen“. (Schlemmer, 1996).

10.4 Accuracy, precision, stability and hysteresis.

Although the sensor presented has been designed to be deployed in a group, and there is not objective related with the design of a high performance sensor, the improvement of the sensor characteristics must drive the design and manufacturing. Important characteristics such as accuracy, precision, stability vs. disturbances (undesirable variables) and hysteresis became relevant for the success of the sensor. The reliability of the sensor and the analyzed application has to match very well.

“Measurements related to product quality are an essential part of quality control systems. Such measurements are directly related to product development where they take the form of dimensional measurements, or they may indirectly affect product quality, where they take the form of processing temperatures. In either case, accuracy in such measurements is mandatory, and to achieve this accuracy, calibration of the instruments used to obtain the measurements must be carried out at a predetermined frequency”. (Morris, 1997).

10.5 Change of the performance in time.

At the beginning, the design of the sensor did not consider the performance of each component with respect to time. Critical issues in the components could be reduced or avoided by a projection of the performance under stress cycling or temperature variations. The cracking or variation of the components from their ideal performance in time could be reduced considerably following some design rules. For example, the design of smoother geometries at the surface of the ring could reduce the cracking for micro fractures which variant the mechanical performance and stress transmission of the sensor body. Humidity, on the other hand, could induce changes into the mechanical performance of the adhesive because of structural molecular variations. Then some design considerations are needed to protect the whole functionality of the sensor.

“Changes in instrument characteristics are related by factors such as mechanical wear, and the effects of dirt, dust, fumes and chemicals in operation environment. When calibration is carried out for quality assurances purposes, it is important that all elements used in the measurement chain are calibrated to produce a quality measurement. Periodic recalibration is necessary because the characteristics of any measuring instrument change over the period of time and affect the relationship between the input and the output”. (Morris, 1997).

10.6 Mechanical uncertainty and other components.

One of the most critical aspects is the quantity of components. More components mean more decoupling singularities and more non-linearities. It is important to initiate a synthesis process to reduce more parts into one, for example the mechanical coupling between the inside support of the sensor body and the fest axis or mechanical earth.

Symmetry is a crucial parameter for the sensor operation, hence the choice of the material, boundaries and manufacturing are quite important. It is recommended to assure a high precision manufacturing.

It is inadequate to consider any assumptions about the homogeneous material of the aluminum. This could produce variations into the mechanical performance,

what can be demonstrated by the finite element analysis. It is important to ensure standardized properties of the sensor body's material.

10.7 Piezoresistive strain gauges.

Adhesive layer is a critical issue to ensure the same performance of the epoxy due to the same rigidity. It is also important to assure the exact position and orientation of the strain gauges. It is recommended to build some marks on the surface of the aluminum to avoid errors during the positioning process.

10.8 Adhesive fracture and cohesive fracture.

In order to prevent the mechanical cohesive performance it is mandatory to have some consideration in a) the design of the sensor body to avoid stress concentrators, b) observe the temperature cycling, and c) observe the humidity under working conditions. To obtain the best performance of the epoxies, enhanced mechanical interlocking and assure the quality of the bonding it is required a profound attention to:

- a. The Cleaning of surface, forming a highly chemically reactive surface for the best intermolecular interlocking - increasing W .
- b. The mechanical abrasion or chemical etching to increase the bonding surface by roughing the surface *-increasing W as well.*

“The small scale contacts and very smooth surfaces associated with information storage devices result in adhesive forces playing a more significant role than in more conventional tribological applications” (Bennett, 1974).

Moreover, it would be very desirable to have a deep understanding of the viscoelastic contact mechanics and the adhesion mechanics. This will reduce the unknown performance of the sensor.

10.9 Hysteresis:

Hysteresis is produced by two elements a) the mechanical coupling of the internal support and the ring and the pre-stressed states of the bonded strain gauges

It is important to measure the temperature of the aluminum surface to determine the stress before the adhesive fixes the strain gauges. This will avoid the failure of pre-stressed strain gauges. In the case that strain gauges 1 or 2 in figure 61 were in a different position of the slope, they would reach the limitations of their performance at different moments.

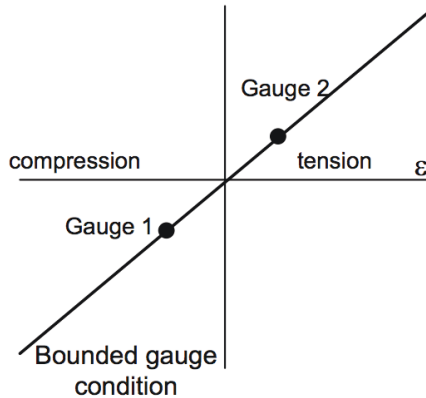


Fig. 61: Pre-strain of the gauges.

10.10 Sensor's performance:

The prototype produces different performance due the mechanical coupling with e.g. the holder that inhibits the high sensibility of the sensor.

The sensor shows an error = 19.3 mV at FSO. This brings an inaccuracy about of the FSO. It is possible to improve this value defining the quantity, quality and performance of the imprecision sources. In this case the most important source was at the montage of each strain gauge because of three main reasons, a) for the absence of the assurance procedure for bonding procedure to determine the exact position and orientation of each strain gauge, b) for the mechanical montage of the intern support

of the ring (the cross) with the geometrical ring and c) for the differences on the adhesive layer at each position of the surface. With some mechanical design modifications it is possible to avoid or reduce these positioning errors at the montage of the strain gauges. The sensor body could have printed the exact position of the gauges. This mechanical coupling inaccuracy could be reduced under a synthesis analysis to reduce the components from two parts into sensor body of one piece.

The value of inaccuracy was under 10 %, like expected. It is possible to reduce this value principally by the improving the accuracy of the montage of the strain gauges.

Even under various mechanisms to protect the degradation of the transducer and sensor body, mechanical and electrical failure will affect sensor performance. Two types of mechanical failure are considered for this sensor, a) Fatigue for the interconnected components, which is caused by mechanical-thermal cycling, and b) Cracking of the sensor packing produced by difference in the thermal expansion coefficients and the packing material. This failure mechanism would weaken the montage of the inside support (cross), and the performance of the adhesive in two regions, with the strain gauges and with the aluminum surface. The cycling of changes in stress and in temperature (cycling life) should be higher than that of the wires (Expertise, 1997).

11. Conclusion

Applications and outlook

Sensor technology should be oriented to the fulfillment of the requirements of new applications in industry, and probably be based on technology oriented to market (Business, 2010). It is our deep desire that this sensor finds a place in industrial and automotive applications.

“There is a market trend towards the use of intelligent sensors. In the past the main reasons for this have been increased measurement accuracy, programmability, decreased inventory cost from the larger turndown available, and a decreased maintenance cost for self-diagnostics.” (Expertise,1997).

“Buyers are showing a marked preference for those types of sensors which are easier to use (Scott, 1995) (Schatz, 2004). This is not shown, nor only in the trend towards intelligent sensors, but also towards those sensors which are easier to install and maintain. (Expertise, 1997).

The use of sensors in cars is producing a growth in the automotive sensors market; all commentators agree on considerable volume growth in the future” (Expertise). “Sensor applications in the automotive segment of the market are without a doubt the largest current and near future applications of sensors. The automotive design-cycle is typically 3-5 years. Several major designs require a large amount of dedicated engineering and design resource”. (Soloman, 1998)

“The automotive industry has been specifically chosen to describe sensor applications for two reasons: it represents an extremely harsh environment for electronic components (Johnson, 2004), and it provides high-volume applications that in turn drive the development of new sensing signals. The automotive environment is recognized to be one of the more difficult applications for electronic systems and micro-electronic sensors. The environment includes a wide temperature range, high-humidity conditions, and the need to withstand several chemicals, operate under high electromagnetic interference. At the same time, the acceptance of electronics is extremely customer driven, it demands low cost and high reliability.” (Ristic, 1994).

Bibliography

- Adam, W.** (2000). Zukunftweisende Anwendungen integrierter Sensorsysteme. VDI-Verlag, Düsseldorf.
- Baumann, P.** (2006). Sensorschaltungen. Vieweg Verlag, Braunschweig.
- Bennett, S.;** Devries, K.L.; Williams, M.L. (1972). Adhesive fracture Mechanics. International Journal of Fracture, vol. 10. no.1.
- Brasche, G.** (2008). Trends and Challenges of Wireless Sensor Networks. ASWN 2008. Eight International Workshop on Applications and Services in Wireless Network, pp. 7.
- Business, W.** (2010, October 13). Research and Markets Global sensors Market in Consumer Electronics. Business Wire.
- Cho, C. J.** (2008). Experimental characterization of the temperature dependence of the piezoresistive coefficients of silicon. IEEE Sensors Journal 8(8), 928-935.
- D'Amico, A.,** & Di Natale, C. (2001). A contribution on some basic definitions of sensor properties. Sensors Journal, vol. 1 no.3, pp.183-190.
- Dario, P.,** Carroza, M., & Guglielmelli, E. (2005). Robotics as a future and emerging technology: biomimetics, cybernetics and neuro-robotics. Robotics & Automation Magazine, vol. 12 no. 2, pp. 29-45.
- D'Ascoli, F.,** Tonarelli, M., & Melani, M. (2005). Intelligent sensor interface for automotive applications., ICECS 2005, 12th IEEE International Conference on Electronic, Circuits and Systems, pp. 11-14.
- Dethe, C.,** Wakde, D., & Jaybhaya, C. (2007). Bluetooth Based Sensor Networks Issues and Techniques., 2007. AMS'07. First Asia International Conference on Modelling & Simulation, pp. 27-30.
- Didden, D.** (1995). Design of a ring-shaped three-axis micro force/torque sensor. Sensors and actuators. A: Physical, vol. 1, Issues 1-3, pp. 225-232.
- Edsinger, A.,** & Kemp, C. (2006). Manipulation in Human Environments, pp. 102-109.

- European Centres of Expertise.** (1997). Sensors. Metra Martech, 5th Edition.
- Fang, B.;** Kempe, D.; Govindan, R. (2006). Utility based sensor selection. The Fifth International Conference on Information Processing in Sensor Networks, pp.11-18.
- FANUC, U. C.** (1994). Patent No. 5,490,427, United States of America.
- Göpel, W.** (2000). From electronic to bioelectronic olfaction or from artificial “moses” to real noses. Sensor and Actuators B, vol. 65, Issues 1-3, pp. 70-72.
- Grandke, T.** (1989). Sensors Volume 1: Fundamentals. Wiley-VCH, pp. 1-16.
- Thomas, W. H.** (1989). Sensors, A Comprehensive Survey, Volume 1, Fundamentals and General Aspects. pp. 135-142.
- Griffith, A.** (1921). The Phenomena of Rupture and Flow in Solids. Philosophical Transactions of the Royal Society of London. Series A, vol. 221, pp. 163-198.
- Hatamura, Y.** (1989). A Ring Shape 6-Axis Force Sensor and its applications. International Conference on Advanced Mechatronics, Tokyo, Japan. pp. 647-652.
- Helfrick, A. D.** (1990). Modern Electronic Instrumentation and Measurement Techniques. Prentice Hall International Editions, pp.197-210
- Hennion, B., & Guinot, J. C.** (2006). Biological inspiration for the conception of virtualquadruped. 489-494. International Conference on Biomedical Robotics and Biomechatronics, pp. 20-22.
- Hwang, B., & Moo, H.** (2009). Monitoring method of interactive toque between humanand robot in exoskeleton systems. International Conference on Rehabilitation Robotics, pp. 23-26
- Israelachivili, J.** (1985). Intermolecular and surface forces.Third edition, ed. Elsevier, pp. 237-239
- Jae, C., Senanayake, S., & Gouwanda, D.** (2009). Precision smart force platform.IEEE/ ASME International Conference on Advanced Intelligent Mechatronics, 2009. AIM 2009, pp. 14-17.

- Jeffrey, H.** (2008). Mathematical Description of Biological Structures and Mechanism. Proceedings of the International Conference on Biocomputation, Bioinformatics, and Biomedical Technologies, pp. 100-108.
- Johnson, R.W.;** Evans, J.L.; Jacobsen, P.; Thompson, J.R.; Christopher M., (2004). The changing automotive environment: high temperature electronics. Transactions on Electronics Packaging Manufacturing, vol. 27, no. 3, pp. 164-176.
- Johnson, K.L.** (1998). Mechanics of adhesion. Tribology International, vol. 31, Issue 8, pp. 413-418
- Juckenack, D.** (1990). Handbuch der Sensortechnik. Messen mechanischer Grössen. Verl. Moderne Industrie Verlag, pp 87-91
- Kanoun, O.,** & Trankler, H.-R. (2004). Sensor Technology advances and future-trends. IEEE Transactions on Instrumentation and Measurement, vol.53, no. 6, pp. 1497-1501.
- Kendall, K.** (1994). Adhesion: Molecules and Mechanics. Science 25, vol. 263, no. 5154, pp. 1720-1725
- Kreuzer, M.** (2004). Linearity and Sensitivity Error in the Use of Single Strain Gauge with Voltage-Fed and Current-Fed Circuits. Experimental Techniques, vol. 8. Issue 10, pp. 30-36.
- Kuwahara, M.,** & Kawaji, S. (2006). Some Remarks on Optimal Sensor Selection Problem. SICE-ICASE, 2006. International Join Conference, pp. 93-98.
- Laschi, C.,** Mazzolai, B., & Patene, F. (2006). Design and Development of a Legged Rat Robot for Studying Animal-Robot Interactions. Biomedical Robotics and Biomechatronics, pp. 631-636.
- Le, Q.,** Kamm, D., & Kara, A. (2010). Learning to grasp objects with multiple contact points. IEEE International Conference on Robotics and Automation (ICRA), 2010, pp, 5062-5069.
- Li Jun;** Meyyappan M. (n.d.). Biomolecular Sensing for cancer diagnostics using carbon nano tubes. BioMEMS and Biomedical Nanotechnology, pp. 1-17

Liang, Q., & Zhang, D. (2009). A novel Miniature Four-Dimensional Force/Torque Sensor with Overload Protection Mechanism. *Sensors Journals*, vol.9, no. 12, pp. 1741-1747

Lind, R., & Love J, L. (2009). Multi-Axis Foot Reaction Force/Torque Sensor for Biomedical Applications. *International Conference on Intelligent Robots and Systems*, pp.2575-2579

Luo, M. H.; Huang, Q. (2008). A Mathematical Model of Six-Axis Force/Moment Sensor and Its applied Control Method for Robot Finger. *Proceedings of the, International Conference on Robotics and Biomometrics*, pp. 1960-1965

Mämpel, J., Koch, T., & Köhring, S. (2009). Concept of a modular climbing robot. *Symposium on Industrial Electronics and Applications*, vol. 2, pp. 789-794.

Marcincin, J. N.; Karnik, L.;Niznik, J. (1997). Design of the intelligent robotics systems from the biorobotics point of view. *International Conference on Intelligent Engineering Systems*, pp. 123-128.

Mon, Y. B.; Lee, J. Y.; Park, S. (2008). Sensor Network Node Management and Implementation. *International Conference on Advanced Communication Technology*, vol. 2, pp. 1321-1324.

Morris, A. S. (1997). *Measurements and calibration requirements*. Ed. John Wiley, pp. 121-128

Nakazawa, N., Uekita, Y.;Onnoka, H.;Ikeru, R., (1996). Experimental study on human's grasping force. *5th IEEE International Workshop on Robot and Human Communication*, pp. 280-285.

Perrin, J. (1923). *Atoms*. Hammick, pp. 109-132.

Peter, V., H.; Liedtke, C.; Droog, E.; van der Kooij, H. (2005). Ambulatory Measurement of Ground Reaction Forces. *IEEE Transactions on Neural Systems and Rehabilitation Engineering*, vol.13, no. 3, pp. 423-427.

Potter, R. W. (2000). *The art of the measurement. Theory and practice*. Prentice Hall PTR, pp. 64-75.

- Qiakang Liang;** Dan Zhang; Quanjun Song; (2010). A potential 4-D Fingertip Force Sensor for an Underwater Robot Manipulator. *IEEE Journal of Oceanic Engineering*, vol.35, no. 3, pp. 574-583.
- Rajaravivarma, V.,** & Yang, Y. (2003). An overview of Wireless Sensor Network and applications. *Proceedings of the 35 the Southeastern Symposium on System Theory*, pp. 432-436.
- Ristic, L.** (1994). *Sensor Technology and devices*. Ed. Artech House Inc., pp. 418-421.
- Robert Dunsch, J.-M. B.** (2006). Unified mechanical approach to piezoelectric bender modeling. *Sensors and Actuators A Physical*, vol.134, pp.436-446.
- Romero, J.;** Kjellström, H.;Kragic, D.,. (2010). Hands in action: real-time 3D reconstruction of hands in interaction objects. *IEEE International Conference on Robotics and Automation (ICRA) 2010*, pp. 458-463.
- Schanz, G. W.** (2004). *Sensoren. Sensortechnik für Praktiker*. Hüttig, pp. 49-60
- Schatz, O.** (2004). Recent trends in automotive sensors. *Sensors, 2004. Proceedings of IEEE*, pp. 236-239.
- Schlemmer, H.** (1996). *Grundlagen der Sensorik. Eine Instrumentenkunde für Vermessungsingenieure*. Wichmann, pp. 204-218.
- Scott, M.** (1995). Sensors- the cost of ownership Monitoring, *IEEE Colloquium on Optical Techniques for Environmental*, pp. 4/1-4/5.
- Sekiguchi, K.;** Ueda, M.; Uno, H.; Takemura, H.; Mizoguchi, H. (2009). Development and calibration of 6-axis force sensor for simultaneous measuring of plantar deformation. *IEEE International Conference on Cybernetics*, pp. 3138-3142.
- Selberherr, S.** (1984). *Analysis and Simulation of Semiconductor Devices*. Ed. Springer Verlag, pp. 118-121
- Sen, A.,** Das, N.; Zhou, L.; Bao, Hong Shen; Murthy, S.;Bhattacharya, P. (2007). Coverage Problem for Sensors Embedded in Temperature Sensitivity Environments.. *4th Annual IEEE Communications Society Conference on Sensor Mesh and Ad Hoc Communications and Networks*, pp. 520-529.

Shimizu, S.; Shimojo, M.;Sato, S; Seki, Y.; Takahashi, A. (1996). The relation between human grip types and force distribution pattern in grasping. 8th International Conference on Advanced Robotics, pp.299-304.

Singh, J. (2004). Development trends in the sensor technology. IEEE Sensor Journal, vol. 5, no. 5, pp. 664-669.

Soloman, S. (1998). Sensors Handbook. Ed. McGraw Hill, pp. 142-154

Tabib Azar, M. (1985). Sensors. Set: A Comprehensive Sensor Survey. Chapter 2. Sensor Parameters.

Taylor, H. R. (1997). Data acquisition for sensor systems. Chapman and Hall, pp. 18-34

Taylor, M., & Chen, X. (2008). TigBot- A wall Climbing Robot for TIG Welding of Stainless Steel Tanks. 15th International Conference on Mechatronics and Machine Vision in Practice, pp. 550-554.

Tränkler, H.-R. (1998). Sensortechnik: Handbuch für Praxis und Wissenschaft. Springer, Berlin-NY-Tokyo.

Veeramachaneni, K., & Osadciw, L. (2008). Swarm intelligence based optimization and control decentralized serial sensor networks. Swarm Intelligence Symposium, SIS 2008. pp. 1-8

Waki, K.; Iwan, T.; Matsunaga, T.;Shimada, Y.;Obinata, G. (2009). Gait estimation using foot-pressure sensors. International Symposium on Micro-NanoMechatronics and Human Science, pp. 62-67.

Webster, J. G. (1998). The measurement instrumentation and sensor handbook. Ed. CRC

Wilson, J. S. (2005). Sensor Technology Handbook. Ed. Newnes,

Window, A. L. (1992). Strain gauge technology. Ed. Elsevier Applied Science,

Witte, H.; Lutherdt, S.; & Schilling, C. (2004). Biomechatronics: how much biology does the engineer need? Proceedings of 2004 IEEE International Conference on Control Applications, vol.2, pp. 944-948.

Wu, B.;Zhongcheng Wu;Fei Shen (2010). Research on calibration system error of 6-axis force/torque sensor integrated in humanoid robot foot. 8th World Congress on Intelligent Control and Automation, pp. 6878-6882.

Yantao, S.; Ning Xi; Li, W. J.; Yongxiong Wang, (2008). Dynamic Performance Enhancement of PVDF Force Sensor for Micromanipulation. IEEE International Conference on Intelligent Robots and Systems, pp. 2827-2832.

Yusuke, K. T. (2003). A directional deflection sensor beam for very small Force/Torque Measurement. International Conference on Intelligent Robots and systems, vol. 2, pp. 1056-1061.

Zatorre, G., Medrano, N.; Sanz, M. T.; Martinez, P.; (2007). Robust Adaptive Electronics for Sensor Conditioning. IEEE Sensors, pp. 1295-1298.

Appendix A

Example of Calibration Matrix

A is the matrix of the values from the six Wheatstone bridges $b_1, b_2, b_3, b_4, b_5, b_6$

$$A = \begin{bmatrix} 8.040 & 1.306 & 6.219 & 1.458 & 6.719 & 8.809 \\ 8.120 & 1.845 & 8.139 & 1.430 & 7.980 & 11.96 \\ 10.97 & 7.379 & 1.072 & 6.901 & 3.898 & 2.416 \\ 2.686 & 1.722 & 1.285 & 1.072 & 1.606 & 0.401 \\ 2.634 & 1.727 & 0.533 & 1.136 & 1.759 & 0.681 \\ 0.257 & 0.170 & 0.7126 & 0.073 & 0.632 & 0.921 \end{bmatrix}$$

The matrix A must satisfy two conditions to determine if $\{b_1, \dots, b_6\}$ is a basis of the space solution of the values from the forces and moments, the space W. According to (Dym 2006)

1. the span $\{b_1, \dots, b_6\} = W$ meaning that the number of vector b must be equal than $\dim W = 6$.
2. The vectors $\{b_1, \dots, b_6\}$ must be linearly independent.

If it is applied the determinant to matrix A :

$$\det(A) = -18.440 \neq 0$$

meaning that the vectors $\{b_1, \dots, b_6\}$ are linearly independent and they serve as a basis of the space solution W, meaning that is possible to build a system in the forma $Ax = F$.

If A is invertible the system has a unique set of scalars $x_i \in W$ with the basis $\{b_1, \dots, b_6\}$

Applying the *inv* (A) we obtain:

$$A^{-1} = \begin{bmatrix} -0.177 & 0.383 & -0.041 & 0.294 & -0.07 & -3.250 \\ -1.348 & 1.236 & -0.109 & 0.490 & 0.603 & -3.532 \\ 0.114 & -0.140 & 0.029 & 0.967 & -1.133 & 1.060 \\ 1.400 & -1.567 & 0.358 & -0.631 & -0.976 & 7.011 \\ 0.832 & -0.944 & -0.085 & -0.645 & 0.987 & 4.078 \\ -0.473 & 0.545 & 0.039 & -0.429 & 0.185 & -1.529 \end{bmatrix}$$

proving that exist a unique set of scalars x_i that resolves the system $A x = F$.

If we resolve the system with

$$F = \begin{bmatrix} 5 \\ 5 \\ 5 \\ 5 \\ 5 \\ 5 \end{bmatrix}$$

we obtain the following values of

$$x = \begin{bmatrix} -14.316 \\ -13.287 \\ 4.498 \\ 27.973 \\ 21.112 \\ -8.304 \end{bmatrix}$$

as a vector solution to this system.

Theses

Titel: Development of biomechatronic devices for measurement of wrenches occurring in animal and human prehension

Author: Omar Eduardo Jiménez López

1. It is achievable to create a specialized sensor to measure forces and moments used for human grasping.
2. The description with precision of the forces and the moments involved in the grasping actions could produce fundamental knowledge for designing ergonomic devices.
3. It is achievable to develop a miniature force-moment sensor node with 6 degrees of freedom (Forces in direction $\langle x, y, z \rangle$ and Moments in direction $\langle x, y, z \rangle$) with a margin error less than $\pm 5\%$.
4. It is achievable to integrate i²c communication among the nodes for transferring the spatial force-moment of the grasping actions from each sensor to the processing unit (master).
5. It is achievable to develop a force-moment sensor node arrangement with blue-tooth capabilities.
6. Feasible technologies for the design of the force-moment sensors are strain gauges and optical solution (hybrid sensor body).
7. Volumetric and multi-node sensing could give a high resolution force-moment mapping from grasping actions.
8. It is feasible to develop a sensor's body with selective strain sensitivity.
9. It is feasible to design a sensor body's geometry with low mechanical distortion produced by the transverse sensitivity.
10. It is achievable to reduce the temperature distortion with dummy strain gauges.

11. It is achievable to develop a hybrid sensor body to combine piezoresistive strain gauges and optical devices.
12. It is feasible to obtain simplicity to the calibration system for the force-moment sensor node traceable to some force standard.
13. It is realizable to develop free maintenance sensor housing.

